Inorg. Chem. **2007**, *46*, 328–340

Aluminum and Zinc Complexes Based on an Amino-Bis(pyrazolyl) Ligand: Synthesis, Structures, and Use in MMA and Lactide Polymerization

Bing Lian,[†] Christophe M. Thomas,[†] Osvaldo L. Casagrande Jr.,[§] Christian W. Lehmann,[||] Thierry Roisnel,[‡] and Jean-François Carpentier*[,†]

Catalyse et Organométalliques, UMR 6226, University of Rennes 1, 35042 Rennes Cedex, France, Centre de Diffractométrie X, Sciences Chimiques de Rennes, Université de Rennes 1, 35042 Rennes, France, Laboratório de Catálise Molecular, Instituto de Quimica-Universidade Federal do Rio Grande do Sul, Av. Bento Gonçalves, 9500, Porto Alegre, RS, 90501-970, Brazil, and Max-Planck-Institut für Kohlenforschung, Chemical Crystallography, Postfach 101353, 45466 Mülheim an der Ruhr, Germany

Received September 14, 2006

The coordination chemistry of bis[2-(3,5-dimethyl-1-pyrazolyl)ethyl]amine (**1**, LH) with aluminum- and zinc-alkyls has been studied. Reaction of **1** with AlR_3 affords the adducts [LH]·AlR_3 (R = Me, **2**; Et, **3**), which undergo alkane elimination upon heating to yield the amido complexes [L]AlR_2 (R = Me, **4**; Et, **5**). Reaction of LiO(*i*PrO)C═CMe_2 with **2** proceeds via N–H deprotonation to give Li[L]$AlMe_3$ (**6**), while the former enolate adds to **4** to generate [Me_2C═C(O*i*Pr)OLi]·[L]$AlMe_2$ (**7**). Similarly, the 1:1 reaction of $ZnEt_2$ with **1** gives [LH]·$ZnEt_2$ (**9**), which is transformed into [L]ZnEt (**10**) upon heating. When an excess of $ZnEt_2$ was used in the latter reaction, the bimetallic complex [L]ZnEt·$ZnEt_2$ (**11**) was isolated beside **10**. Performing the same reaction in the presence of O_2 traces yielded selectively the dinuclear ethyl-ethoxide complex [L]$Zn_2Et_2(\mu$-OEt) (**12**), which was alternatively prepared from the reaction of **10** and ZnEt(OEt). Zinc chloride complexes [LH]·ZnRCl (R = Et, **13**; *p*-$CH_3C_6H_4CH_2$, **14**) and [L]ZnCl (**15**) were prepared in high yields following similar strategies. Ethyl abstraction from **10** with $B(C_6F_5)_3$ yields [L]$Zn^+EtB(C_6F_5)_3^-$ (**16**). All complexes have been characterized by multinuclear nuclear magnetic resonance (NMR), elemental analysis, and single-crystal X-ray diffraction studies for four-coordinate Al complexes **2**, **4**, and **6** and Zn complexes **9**–**12** and **14**. Aluminate species **6** and **7** initiate the polymerization of methyl methacrylate, and the monomer conversions are improved in the presence of neutral complexes **2** or **4**, respectively; however, these methyl methacrylate (MMA) polymerizations are uncontrolled. Polymerization of *rac*-lactide takes place at 20 °C in the presence of zinc ethoxide complex **12** to yield atactic polymers with controlled molecular masses and relatively narrow polydispersities.

Introduction

The chemistry of alkyl-aluminum derivatives bearing nitrogen-based bidentate or tridentate ligands has recently attracted much attention because of the rich structural chemistry of this class of complexes[1] and their applicability as unique catalysts in fine chemical synthesis[2] and even more in olefin polymerization.[3] Such neutral or cationic species have the potential to function as very active catalysts because of their less coordinatively saturated nature, as compared to more usual tetradentate (e.g., SALEN) ligated complexes. Aluminum-based initiators are also of great utility for the

* To whom correspondence should be addressed. Fax: (+33)(0)223-236-939. E-mail: jean-francois.carpentier@univ-rennes1.fr.
[†] Université de Rennes 1.
[‡] Centre de Diffractométrie X, Rennes.
[§] Universidade Federal do Rio Grande do Sul.
[||] Max-Planck-Institut für Kohlenforschung.

(1) (a) Trepanier, S. J.; Wang, S. *Angew. Chem., Int. Ed. Engl.* **1994**, *33*, 1265−1266. (b) Trepanier, S. J.; Wang, S. *Organometallics* **1994**, *13*, 2213−2217. (c) Trepanier, S. J.; Wang, S. *J. Chem. Soc., Dalton Trans.* **1995**, 2425−2429. (d) Trepanier, S. J.; Wang, S. *Can. J. Chem.* **1996**, *74*, 2032−2040. (e) Lewinski, J.; Zachara, J.; Mank, B.; Pasynkiewicz, S. *J. Organomet. Chem.* **1993**, *454*, 5−7.
(2) (a) Ooi, T.; Maruoka, K. *Lewis Acids in Organic Synthesis*; Yamamoto, H., Ed.; Wiley-VCH: Weinheim, Germany, 2000; Vol. 1, pp 191−281. (b) Wulff, W. D. *Lewis Acids in Organic Synthesis*; Yamamoto, H., Ed.; Wiley-VCH: Weinheim, Germany, 2000; Vol. 1, pp 283−354.

10.1021/ic061749z CCC: $37.00
Published on Web 11/23/2006

Scheme 1

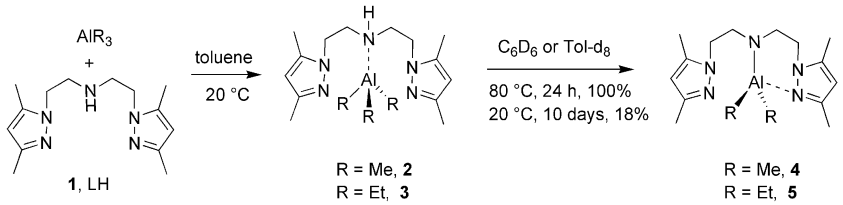

controlled polymerization of polar monomers such as (meth)-acrylates, propylene oxide, and lactones, and alkyl-aluminum complexes bearing tridentate nitrogen ligands designed for this purpose have been recently disclosed.[4] A few zinc complexes of tridentate nitrogen donor ligands have also been prepared, mostly to study their coordination chemistry,[5] for example, as models of metalloenzymes.[6] A large number of those tridentate N,N,N-ligated Al and Zn complexes include neutral pyridine-2,6-diimine or monoanionic pyrroyl-2,5-diimine ligands. This type of framework is nowadays ubiquitous to all coordination/catalysis chemists since the discovery of highly active iron and cobalt ethylene polymerization catalysts derived from such bulky tridentate pyridine-diimine ligands.[7]

Recently, we have reported the synthesis of amino-bis(pyrazolyl) ligands as new readily available tridentate N,N,N-ligands for the nickel-catalyzed selective dimerization of ethylene to 1-butene.[8] We found also that this class of ligands is very valuable for the chromium-catalyzed oligomerization of ethylene.[9] As an extension of our continuous interest in this field, we have investigated the reactions of trialkylaluminum and dialkylzinc with bis[2-(3,5-dimethyl-1-pyrazolyl-)ethyl]amine (**1**, LH), which can act as a neutral or monoanionic ligand. We selected this tridentate ligand because of its potential ability to stabilize both neutral and cationic metal centers, having in mind that tridentate amine or amidoamine initiators have shown remarkable performance in polymerization of polar monomers, though only a few of them have been investigated thus far.[4] We report in this paper the syntheses, structures, and reactivity of a series of mononuclear and dinuclear complexes as well as applications of some of these derivatives in the addition and ring-opening polymerization of methyl methacrylate and lactide.

Results and Discussion

Synthesis and Structure of Neutral Aluminum Complexes Supported by Tridentate Ligand Bis[2-(3,5-dimethyl-1-pyrazolyl)ethyl]amine (1). The reaction of ligand **1** (LH) with 1 equiv of $AlMe_3$ or $AlEt_3$ at room temperature in benzene or toluene affords the corresponding adduct complexes [LH]·AlR_3 (R = Me, **2**; Et, **3**), which were isolated as blocky colorless crystals in high yield (>80%) (Scheme 1). Both complexes **2** and **3** were characterized by elemental analysis and nuclear magnetic resonance (NMR) spectroscopy. The room-temperature ^{1}H NMR spectra in various solvents (benzene-d_6, toluene-d_8, CD_2Cl_2, THF-d_8) and the ^{13}C NMR spectra in C_6D_6 of **2** and **3** show all a single set of resonances for a symmetrically coordinated ligand and three magnetically equivalent Al−R (R = Me, Et) groups. Coordination of **1** via the central *N*H atom in **2** was confirmed by single-crystal X-ray diffraction, the result of which is shown in Figure 1, together with a selection of bond lengths and angles. The solid-state structure of **2** shows the Al center in a four-coordinated geometry with the two pyrazolyl groups pointing in opposite directions from the Al center.

Methane and ethane elimination from complexes **2** and **3**, respectively, takes place slowly at room temperature in aromatic hydrocarbons. Heating **2** and **3** at 80 °C for 24 h gave the corresponding amido-dialkyl complexes [L]AlR_2 (R = Me, **4**; Et, **5**) in quantitative NMR yield (Scheme 1). Complex **4** was isolated as colorless crystals and was fully characterized by elemental analysis, NMR spectroscopy, and X-ray diffraction analysis; the parent diethyl complex **5** was generated on an NMR scale. The solid-state structure of **4** (Figure 2, Table 1) shows that only one pyrazolyl moiety is coordinated to the Al center, which illustrates again the strongly favored formation of four-coordinated Al species.[10]

(3) (a) Coles, M. P.; Jordan, R. F. *J. Am. Chem. Soc.* **1997**, *119*, 8125−8126. (b) Coles, M. P.; Swemson, D. C.; Jordan, R. F.; Young, V. G., Jr. *Organometallics* **1997**, *16*, 5183−5194. (c) Ihara, E.; Young, V. G., Jr.; Jordan, R. F. *J. Am. Chem. Soc.* **1998**, *120*, 8277−8278. (d) Radzewich, C. E.; Coles, M. P.; Jordan, R. F. *J. Am. Chem. Soc.* **1998**, *120*, 9384−9385. (e) Aeilts, S. L.; Coles, M. P.; Swenson, D. C.; Jordan, R. F.; Young, V. G., Jr. *Organometallics* **1998**, *17*, 3265−3270. (f) Coles, M. P.; Swenson, D. C.; Jordan, R. F.; Young, V. G., Jr. *Organometallics* **1998**, *17*, 4042−4048. (g) Bruce, M.; Gibson, V. C.; Redshaw, C.; Solan, G. A.; White, A. J. P.; Williams, D. J. *Chem. Commun.* **1998**, 2523−2524. (h) Radzewich, C. E.; Guzei, I. A.; Jordan, R. F. *J. Am. Chem. Soc.* **1999**, *121*, 8673−8674. (i) Korolev, A. V.; Guzei, I. A.; Jordan, R. F. *J. Am. Chem. Soc.* **1999**, *121*, 11605−11606. (j) Dagorne, S.; Guzei, I. A.; Coles, M. P.; Jordan, R. F. *J. Am. Chem. Soc.* **2000**, *122*, 274−289. (k) Korolev, A. V.; Ihara, E.; Guzei, I. A.; Young, V. G., Jr.; Jordan, R. F. *J. Am. Chem. Soc.* **2001**, *123*, 8291−8309. (l) Matsuo, Y.; Tsurugi, H.; Yamagata, T.; Tani, K.; Mashima, K. *Bull. Chem. Soc. Jpn.* **2003**, *76*, 1965−1968.
(4) (a) Emig, N.; Nguyen, H.; Krautscheid, H.; Réau, R.; Cazaux, J.-B.; Bertrand, G. *Organometallics* **1998**, *17*, 3599−3608. (b) Jegier, J. A.; Atwood, D. A. *Inorg. Chem.* **1997**, *36*, 2034−2039. (c) Saunders, Baugh, L.; Sissano, J. A. *J. Polym. Sci., Part A: Polym. Chem.* **2002**, *40*, 1633−1651.
(5) Luo, B.; Kucera, B. E.; Gladfelter, W. L. *Polyhedron* **2006**, *25*, 279−285 and references cited therein.
(6) See for example: Gosiewska, S.; Cornelissen, J. J. L. M.; Lutz, M.; Spek, A. L.; van Koten, G.; Klein Gebbink, R. J. *Inorg. Chem.* **2006**, *45*, 4214−4227. and references cited therein.
(7) (a) Britovsek, G. J. P.; Gibson, V. C.; Kimberley, B. S.; Maddox, P. J.; Mc Tavish, S. J.; Solan, G. A.; White, A. J. P.; Williams, D. J.; *Chem. Commun.* **1998**, 849−850. (b) Small, B. L.; Brookhart, M.; Bennett, A. M. A. *J. Am. Chem. Soc.* **1998**, *120*, 4049−4050.
(8) Ajellal, N.; Kuhn, M. C. A.; Boff, A. D. G.; Hoerner, M.; Thomas, C. M.; Carpentier, J.-F.; Casagrande, O. L., Jr. *Organometallics* **2006**, *25*, 1213−1216.
(9) Junges, F.; Kuhn, M. C. A; Ajellal, N.; Thomas, C. M.; Carpentier, J.-F.; Casagrande, O. L., Jr. Manuscript in preparation.
(10) (a) Healy, M. D.; Ziller, J. W.; Barron, A. R. *J. Am. Chem. Soc.* **1990**, *112*, 2949−2954. (b) Trepanier, S. J.; Wang, S. *Organometallics* **1996**, *15*, 760−765.

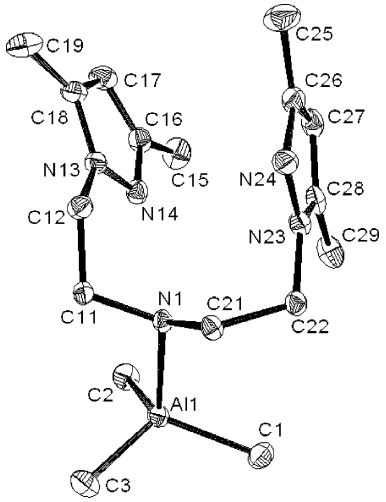

Figure 1. Solid-state structure of **2** (ellipsoids drawn at the 50% probability; hydrogen atoms omitted for clarity). Selected bond lengths (Å) and angles (deg): Al(1)—C(1), 1.9865(12); Al(1)—C(2), 1.9797(13); Al(1)—C(3), 1.9800(15); Al(1)—N(1), 2.0370(11); C(1)—Al(1)—C(2), 114.82(6); C(1)—Al(1)—C(3), 113.47(6); C(2)—Al(1)—C(3), 115.53(5); N(1)—Al(1)—C(1), 105.02(5); N(1)—Al(1)—C(2), 102.45(5); N(1)—Al(1)—C(3), 103.52(5).

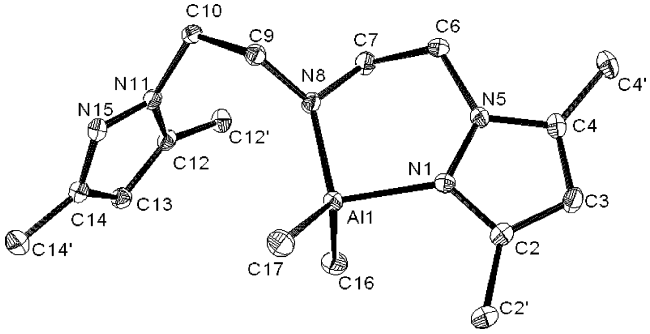

Figure 2. Solid-state structure of **4** (ellipsoids drawn at the 50% probability; hydrogen atoms omitted for clarity). Selected bond lengths (Å) and angles (deg): Al(1)—C(16), 1.9732(13); Al(1)—C(17), 1.9698(13); Al(1)—N(1), 2.0025(10); Al(1)—N(8), 1.8267(10); C(16)—Al(1)—C(17), 117.32(6); C(16)—Al(1)—N(1), 102.06(5); C(16)—Al(1)—N(8), 115.06(5); C(17)—Al(1)—N(1), 111.44(5); C(17)—EnDashAl(1)—N(8), 112.89(5); N(1)—Al(1)—N(8), 95.02(4).

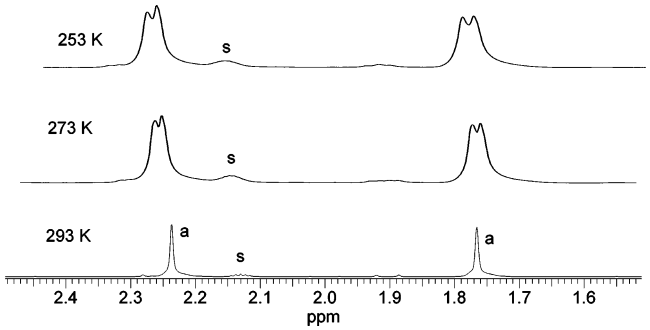

Figure 3. Selected region of the variable-temperature ^{1}H NMR spectra (300 MHz, Tol-d_8) of **4**. Descriptors **a** and **s** refer, respectively, to the CH_3 pyrazolyl groups of **4** and the residual solvent resonances (Tol-d_8).

The Al—N(amido) bond length involving the sp^2-hybridized nitrogen-bridge atom in complex **4** (sum of angles around N(8) = 357.81°; Al—N(8), 1.8267(10) Å) is logically much shorter than the corresponding Al—N(amino) bond length in adduct complex **2** (sum of angles around N(1) = 336.47°; Al—N(1), 2.037(11) Å). The latter is similar to the new Al—N(pyrazolyl) bond length formed in **4** (Al—N(1), 2.0025(10) Å). No difference is observed in the Al—C bond lengths in both complexes (Al—C, 1.9732(13) and 1.9698(13) in **4** vs 1.9797(13) and 1.9800(15) in **2**). The variable-temperature ^{1}H NMR spectrum of **4** in toluene-d_8 solution is also in agreement with a four-coordinated aluminum species (Figure 3): at low temperature (0 °C), four [broadened] singlets are observed for the four inequivalent *Me* pyrazolyl groups, and the two Al—Me groups appear as two singlets. At room temperature, both the free and coordinated pyrazolyl groups exchange fast on the NMR time scale, and the Me pyrazolyl and $AlMe_2$ groups appear as two sharp singlets and one singlet, respectively.

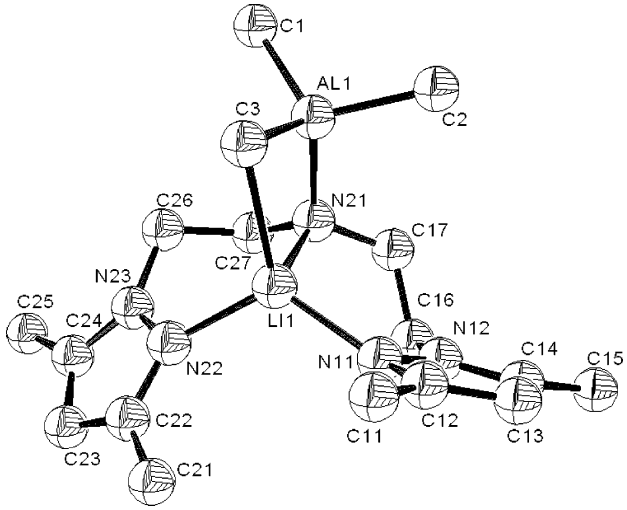

Figure 4. Solid-state structure of **6** (ellipsoids drawn at the 50% probability; hydrogen atoms omitted for clarity). Selected bond lengths (Å) and angles (deg): Al(1)—C(1), 2.001(2); Al(1)—C(2), 1.987(2); Al(1)—C(3), 2.013(2); Al(1)—N(21), 1.9151(19); Li(1)—C(3), 2.395(4); Li(1)—N(21), 2.050(4); Li(1)—N(22), 1.957(4); Li(1)—N(11), 1.985(4); C(1)—Al(1)—C(2), 114.61(10); C(1)—Al(1)—C(3), 109.94(10); C(3)—Al(1)—N(21), 104.98(8); C(2)—Al(1)—C(3), 106.80(9); Al(1)—C(3)—Li(1), 76.29(10); Al(1)—N(21)—Li(1), 87.31(12); C(3)—Li(1)—N(21), 88.69(14).

The preparation of Al-enolate complexes, potentially active species for methyl methacrylate (MMA) polymerization,[11] was attempted following different routes. In the reaction of $AlMe_3$-adduct **2** with 1 equiv of Li-ester enolate LiO(*i*PrO)C=CMe_2, deprotonation of the N—H moiety was found to proceed faster than enolate addition, to give selectively the bimetallic aluminum-lithium amido complex Li[L]$AlMe_3$ (**6**), with concomitant release of 1 equiv of isopropyl isobutyrate (identified by ^{1}H and ^{13}C NMR) (Scheme 2). This pathway was not unexpected considering the enhanced acidity of N—H because of its coordination onto Al (as compared to that of free-ligand **1**). An X-ray diffraction analysis of a single crystal of **6** confirmed its molecular monomeric structure and showed that both Al and Li are in a tetracoordinate environment (Figure 4, Table 1). The Li atom is actually coordinated by the three N atoms of the ligand, thus generating two six-membered metallacycles, via an agostic interaction with one of the Al—*C*H_3 groups. The short contact between lithium and the methyl carbon

(11) Rodriguez-Delgado, A.; Chen, E. Y.-X. *J. Am. Chem. Soc.* **2005**, *127*, 961—974.

Table 1. Crystal Data and Structure Refinement for Aluminum Complexes **2**, **4**, and **6**

	2	**4**	**6**
empirical formula	$C_{17}H_{32}AlN_5$	$C_{16}H_{28}AlN_5$	$C_{17}H_{31}AlLiN_5$
fw/g·mol^{-1}	333.46	317.41	339.39
temperature/K	100(2)	100	373(2)
wavelength/Å	0.71073	0.71073	0.71069
crystal system	triclinic	monoclinic	triclinic
space group	$P\bar{1}$	$P2_1/c$ (no. 14)	$P\bar{1}$
a [Å]	8.8262(4)	13.0200(3)	7.822(5)
b [Å]	10.9199(5)	9.5441(2)	11.327(5)
c [Å]	11.7634(5)	14.5474(3)	12.250(5)
α/deg	112.305(2)	90	83.801(5)
β/deg	93.821(2)	94.8040(10)	78.221(5)
γ/deg	106.374(2)	90	72.077(5)
volume/Å^3	986.95(8)	1801.37(7)	1009.7(9)
Z	2	4	2
density (cacld) Mg·m^{-3}	1.122	1.170	1.116
absorp coeff/mm^{-1}	0.110	0.117	0.108
F(000)	364	688	368
crystal size/mm^3	0.6 × 0.4 × 0.3	0.44 × 0.07 × 0.07	0.7 × 0.4 × 0.2
θ range for data collection/deg	2.66−32.00	2.94−31.02	2.48−27.94
index ranges	$-13 \le h \le 13$ $-16 \le k \le 16$ $-17 \le l \le 17$	$-18 \le h \le 18$ $-13 \le k \le 13$ $-21 \le l \le 21$	$-9 \le h \le 10$ $-14 \le k \le 14$ $-16 \le l \le 16$
reflns collected	22 398	48 457	16 887
indep reflns	6760 [$R_{int} = 0.0302$]	5746 [$R_{int} = 0.0543$]	4677 [$R_{int} = 0.0546$]
absorp correction	semiempirical from equivalents	semiempirical from equivalents	none
refinement method	full-matrix least squares on F^2	full-matrix least squares on F^2	full-matrix least squares on F^2
data /restraints/params	6760/0/212	5746/0/205	4677/0/217
goodness-of-fit on F^2	1.035	1.039	1.060
final R indices[$I > 2\sigma(I)$]	$R_1 = 0.0444$ $wR_2 = 0.1339$	$R_1 = 0.0461$ $wR_2 = 0.1073$	$R_1 = 0.0526$ $wR_2 = 0.1548$
R indices (all data)	$R_1 = 0.0500$ $wR_2 = 0.1409$	$R_1 = 0.0587$ $wR_2 = 0.1140$	$R_1 = 0.0726$ $wR_2 = 0.1654$
largest diff. peak and hole/e·Å^{-3}	0.542 and −0.482	0.378 and −0.321	0.435 and −0.404

Scheme 2

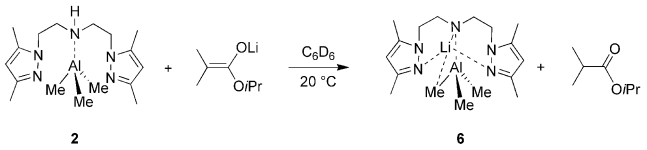

2 **6**

Scheme 3

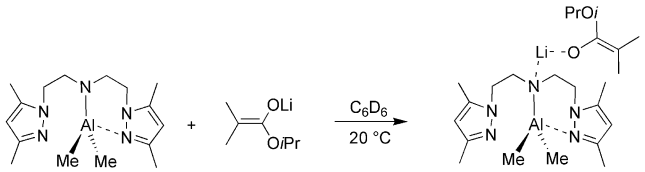

4 **7**

atom (Li—C(3), 2.395(4) Å) falls in the upper range for such Li...Me...Al interactions (2.185−2.36 Å)[12] and generates another four-membered bismetallacycle which is nearly planar (torsion angle Al(1)—C(3)—Li(1)—N(21) = 14.4°). The Al—N bond length involving the tetragonal nitrogen bridge atom in **6** (Al—N(21), 1.9151(19) Å) is intermediary to those found in **2** and **4** (vide supra).

The addition of 1 equiv of Li-ester enolate to dimethylamido complex **4** was monitored by ^{1}H NMR and was found to generate a unique species, [Me_2C═C(O*i*Pr)OLi]·[L]AlMe_2 (**7**, Scheme 3). In the ^{1}H and ^{13}C NMR spectra of **7** in C_6D_6, only some of the resonances for the N-CH_2CH_2 group (δ ^{1}H 3.63 and 3.55, δ ^{13}C 54.43 and 49.69 ppm) are significantly shifted as compared to those of **4** (δ ^{1}H 3.62 and 3.20, δ ^{13}C 51.03 and 49.74 ppm); in particular, the resonances for AlMe_2 are not affected (δ ^{1}H −0.34, δ ^{13}C −8.90 in **7** vs δ ^{1}H −0.31, δ ^{13}C −8.51 in **4**). These observations suggest that aluminate species did not form and only coordination between the Li and N atoms of the ligand takes place in **7**. The formation of aluminate-enolate species is likely hampered by the favorable four-coordination of the Al center in **4**.

An Al-enolate species was obtained by the addition of 1 equiv of 2,4,6-trimethylacetophenone to either complex **2** or **4** (Scheme 4). Methane elimination was not observed in the reaction of **4** with the bulky enolizable ketone, but reprotonation of the N(amido) atom takes place to form [LH]-AlMe_2(OC(2,4,6-Me_3Ph)═CH_2) (**8**) quantitatively within 2 h at room temperature. The same product was obtained from the methane elimination reaction between the trimethylaluminum adduct **2** and 2,4,6-trimethylacetophenone; the kinetics of this reaction are much slower in comparison with the route from **4** (35% conversion after 15 h at room temperature), and a higher temperature is required to go to completion.

Synthesis of Neutral and Cationic Zinc Complexes Supported by Tridentate Ligand Bis[2-(3,5-dimethyl-1-pyrazolyl)ethyl]amine (1). The reaction of ligand **1** with 1

(12) (a) Armstrong, D. R.; Clegg, W.; Davies, R. P.; Liddle, S. T.; Linton, D. J.; Raithby, P. R.; Snaith, R.; Wheatley, A. E. H. *Angew. Chem., Int. Ed.* **1999**, *38*, 3367−3370. (b) Boss, S. R.; Cole, J. M.; Haigh, R.; Snaith, R.; Wheatley, A. E. H.; McIntyre, G. J.; Raithby, P. R. *Organometallics* **2004**, *23*, 4527−4530. (c) Uhl, W.; Layh, M.; Massa, W. *Chem. Ber.* **1991**, *124*, 1511−1516. (d) Fryzuk, M. D.; Giesbrecht, G. R.; Rettig, S. J. *Organometallics* **1997**, *16*, 725−736. (e) Armstrong, D. R.; Davies, R. P.; Linton, D. J.; Snaith, R.; Schooler, P.; Wheatley, A. E. H. *Dalton Trans.* **2001**, 2838−2843.

Scheme 4

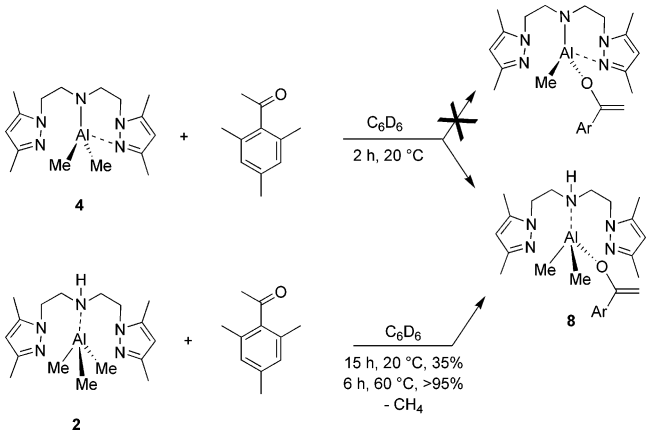

Scheme 5

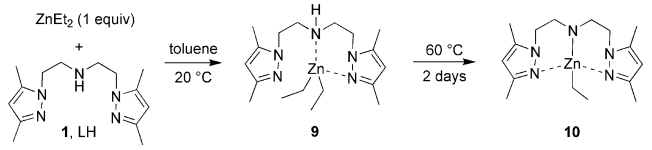

Scheme 6

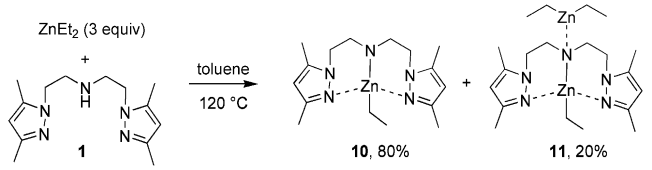

equiv of $ZnEt_2$ in toluene at room temperature gives the adduct complex [LH]·$ZnEt_2$ (**9**) in high yield (90%) (Scheme 5). Heating complex **9** at 60 °C yielded quantitatively the pure anticipated complex [L]ZnEt (**10**), together with release of 1 equiv of ethane (Scheme 5). Initially, we carried out this sequential reaction directly at high temperature, using an excess (3 equiv) of $ZnEt_2$ versus **1**, to drive it to completion. Under these conditions, the amido-ethyl-zinc complex **10** was formed in ca. 80% selectivity beside ca. 20% of bimetallic complex [L]ZnEt·$ZnEt_2$ (**11**), which arises from coordination of an extra $ZnEt_2$ unit to the amide-N atom of **10** (Scheme 6). Obviously, exact stoichiometry must be respected in this reaction to ensure the selective formation of desired complex **10**. Also, when the reaction between ligand **1** and 3 equiv of $ZnEt_2$ was carried out at 120 °C in the presence of traces of O_2, the mixed dinuclear ethyl-ethoxide complex [L]Zn_2Et_2(μ-OEt) (**12**) was recovered in high yield as the only product (Scheme 7). We assume that this reaction proceeds primarily by the formation of **11**, followed by addition of dioxygen in one of the Zn—C bonds and final structural rearrangement.[13] Alternatively, we found that complex **12** can also be readily synthesized by the reaction of **10** with 1 equiv of ZnEt(OEt) (Scheme 7).

The reaction of ligand **1** with 1 equiv of Zn(R)Cl at room temperature cleanly afforded the corresponding zinc adduct [LH]·ZnRCl (R = Et, **13**; *p*-$CH_3C_6H_4CH_2$, **14**) in high yields

Scheme 7

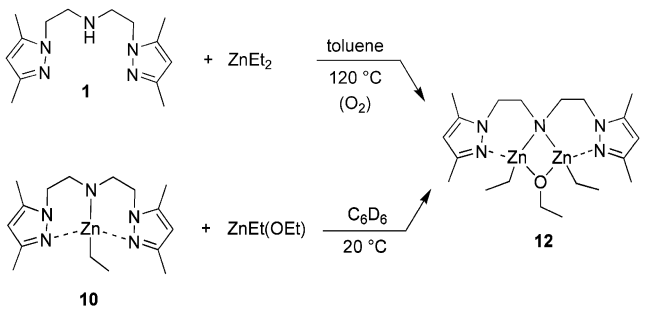

Scheme 8

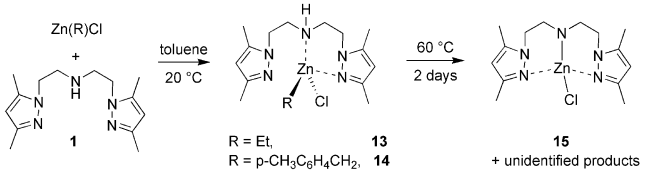

Scheme 9

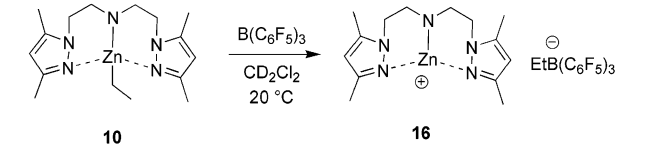

(Scheme 8). Heating **13** at 60 °C (to undergo alkane elimination) yielded a mixture of products, as evidenced by complicated NMR spectra, which could not be fully characterized. Similar treatment of benzylic complex **14** gave the chloride complex [L]ZnCl (**15**) in 86% NMR purity, but some problems were encountered in the final purification.

Finally, the cationic complex [L]Zn^+ $EtB(C_6F_5)_3^-$ (**16**) was cleanly generated in CD_2Cl_2 by abstraction of the ethyl group of **10** with 1 equiv of $B(C_6F_5)_3$ (Scheme 9). This product, which was fully characterized in solution by ^1H, ^{13}C, ^{11}B, and ^{19}F NMR spectroscopy, is stable at least 2 days at room temperature. However, attempts to grow single crystals were unsuccessful.

Structures of Zinc Complexes. Complexes **9**−**12** and **14** have been characterized by single-crystal X-ray diffraction studies. Crystallographic details are reported in Table 2, and the molecular structures as well as selected bond lengths and angles are given in Figures 5−9. With the exception of complex **10** which is dimeric, all the other zinc complexes feature a monomeric structure in the solid state.

The zinc atom in the diethylzinc−adduct **9** presents a distorted tetrahedral geometry with an acute N(pyrazolyl)—Zn—N(bridge) angle (N(1)—Zn(1)—N(3), 86.23(12)°) and

(13) Similar dioxygen addition (adventitious) reactions have been reported: (a) Bailey, P. J.; Dick, C. M. E.; Fabre, S.; Parsons S. *Dalton Trans.* **2000**, 1655−1661. (b) Dove, A. P.; Gibson, V. C.; Hormnirun, P.; Marshall, E. L.; Segal, J. A.; White, A. J. P.; Williams, D. J. *Dalton Trans.* **2003**, 3088−3097. (c) Conway, B.; Hevia, E.; Kennedy, A. R.; Mulvey, R. E.; Weatherstone, S. *Dalton Trans.* **2005**, 1532−1544. (d) Lewinski, J.; Zachara, J.; Gos, P.; Grabska, E.; Kopec, T.; Madura, I.; Marciniak, W.; Prowotorow, I. *Chem. Eur. J.* **2000**, *6*, 3215−3227. (e) Lewinski, J; Sliwinski, W.; Dranka, M.; Justyniak, I.; Lipkowski, J. *Angew. Chem., Int. Ed.* **2006**, *45*, 4826−4829. and references cited therein.

Table 2. Crystal Data and Structure Refinement for Zinc Complexes **9**−**12** and **14**

	9	**10**	**11**	**12**	**14**
empirical formula	$C_{18}H_{33}N_5Zn$	$C_{16}H_{27}N_5Zn$	$C_{20}H_{37}N_5Zn_2$	$C_{20}H_{37}N_5OZn_2$	$C_{22}H_{32}ClN_5Zn$
fw/g·mol^{-1}	384.86	354.81	478.29	494.29	467.35
temperature/K	120(2)	100	100	100(2)	100(2)
wavelength/Å	0.71073	0.71073	0.71073	0.71073	0.71073
crystal system	triclinic	triclinic	monoclinic	triclinic	monoclinic
space group	$P\bar{1}$	$P\bar{1}$ (no. 2)	$P2_1/n$ (no. 14)	$P\bar{1}$	$P21/c$
a [Å]	8.1449(7)	8.9577(2)	8.7921(2)	8.7390(8)	8.675(2)
b [Å]	8.4941(7)	9.2260(3)	28.5056(7)	9.5046(8)	21.637(5)
c [Å]	15.2918(13)	13.0692(4)	9.3278(2)	14.6311(12)	12.645(3)
α/deg	99.522(4)	75.9050(10)	90	83.137(4)	90
β/deg	104.599(4)	80.4720(10)	96.2280(10)	81.479(4)	106.436(12)
γ/deg	97.946(4)	67.0600(10)	90	77.207(4)	90
volume/Å^3	991.57(15)	961.70(5)	2323.97(9)	1167.28(17)	2276.5(10)
Z	2	2	4	2	4
density (cacld) Mg·m^{-3}	1.289	1.360	1.367	1.406	1.364
absorp coeff/ mm^{-1}	1.248	1.288	2.078	2.074	1.214
F(000)	412	418	1008	520	984
crystal size/ mm^3	0.25 × 0.12 × 0.05	0.21 × 0.14 × 0.05	0.18 × 0.10 × 0.05	0.3 × 0.12 × 0.05	0.3 × 0.25 × 0.2
θ range for data collection/deg	5.16−27.65	3.06−31.01	3.07−31.05	2.51−35.22	2.62−27.65
index ranges	$-10 \le h \le 10$ $-11 \le k \le 10$ $-19 \le l \le 19$	$-12 \le h \le 12$ $-13 \le k \le 13$ $-18 \le l \le 18$	$-12 \le h \le 12$ $-41 \le k \le 41$ $-13 \le l \le 13$	$-13 \le h \le 13$ $-14 \le k$ e 15 $-23 \le l \le 23$	$-10 \le h \le 11$ $-28 \le k \le 28$ $-16 \le l \le 16$
reflns collected	7970	24 901	39 812	27 202	28 850
indep reflns	4474 [$R_{int} = 0.0405$]	6098 [$R_{int} = 0.0406$]	7420 [$R_{int} = 0.0582$]	9140 [$R_{int} = 0.0402$]	5221 [$R_{int} = 0.0282$]
absorp correction	none	semiempirical from equivalents	semiempirical from equivalents	semiempirical from equivalents	semiempirical from equivalents
refinement method	full-matrix least squares on F^2	full-matrix least squares on F^2	full-matrix least squares on F^2	full-matrix least squares on F^2	full-matrix least squares on F^2
data/restraints/params	4474/0/220	6098/0/231	7420/0/251	9140/0/253	5221/0/268
goodness-of-fit on F^2	1.153	1.075	1.259	1.016	1.045
final R indices[$I > 2\sigma(I)$]	$R_1 = 0.0585$ $wR_2 = 0.1349$	$R_1 = 0.0291$ $wR_2 = 0.0693$	$R_1 = 0.0781$ $wR_2 = 0.1499$	$R_1 = 0.0416$ $wR_2 = 0.1091$	$R_1 = 0.0260$ $wR_2 = 0.0716$
R indices (all data)	$R_1 = 0.0757$ $wR_2 = 0.1452$	$R_1 = 0.0326$ $wR_2 = 0.0708$	$R_1 = 0.0956$ $wR_2 = 0.1560$	$R_1 = 0.0617$ $wR_2 = 0.1186$	$R_1 = 0.0298$ $wR_2 = 0.0736$
largest diff. peak and hole/ e·Å^{-3}	0.796 and −0.744	0.544 and −0.510	1.927 and −1.288	1.365 and −1.915	0.616 and −0.296

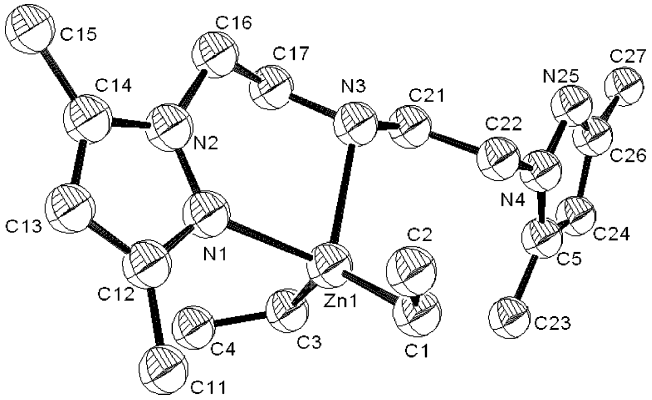

Figure 5. Solid-state structure of **9** (ellipsoids drawn at the 50% probability; hydrogen atoms omitted for clarity). Selected bond lengths (Å) and angles (deg): Zn(1)−C(1), 2.006(4); Zn(1)−C(3), 2.017(4); Zn(1)−N(1), 2.214(3); Zn(1)−N(3), 2.263(3); C(1)−Zn(1)−C(3), 134.78(16); C(1)−Zn(1)−N(1), 106.35(15); C(1)−Zn(1)−N(3), 111.90(14); N(1)−Zn(1)−N(3), 86.23(12).

an opened C−Zn−C angle (C(1)−Zn(1)−C(3), 134.78(16)°) (Figure 5). These values fall in the ranges of those observed for related adducts of $ZnEt_2$ with a four-membered chelating diamine which feature acute N−Zn−N angles but narrower Et−Zn−Et bond angles[14] and those of adducts with two monoamine ligands which have more opened N−Zn−N angles.[15] The Zn−C and Zn−N bond lengths are comparable to those observed in the aforementioned adducts.[14,15]

The solid-state structure of dimeric ethyl-amido complex **10** features also two four-coordinated Zn centers, with μ-bridging via the N atom of the ligand bridge (Figure 6). The overall structure of **10**, centrosymmetric around the square Zn_2N_2 plane, and its geometric features (bond lengths and angles) are reminiscent to other dimeric alkyl-(amino-μ-amido) Zn complexes of general formula $[R^1ZnNR^2(CH_2)_n\text{-}NHR^2]_2$ (R^1 = H, Me, Et; R^2 = Me, Bn; n = 2, 3),[5,16] also prepared from the reaction of ZnR_2[1] with primary diamines.

The molecular structure of dinuclear complex **11** reveals a four-coordinated Zn center in a distorted tetrahedral environment, together with a $ZnEt_2$ unit singly coordinated to the amido-N atom in a planar trigonal geometry (Figure 7). In the latter respect, **11** is a rare example of a structurally characterized trigonal adduct of a dialkylzinc onto a Lewis base.[17] The geometry around the $ZnEt_2$ fragment in **11** (Zn(2)−N(8), 2.100(3); Zn(2)−C(18), 1.988(5); Zn(2)−C(20),1.995(5) Å; C(18)−Zn(2)−C(20), 137.0(2)°) compares remarkably to that of Arduengo's nucleophilic carbene-$ZnEt_2$ adduct (carbene: 1,3-di(1-adamantyl)imidazol-2-ylidene; Zn−C(carbene), 2.096; Zn−C(Et), 1.994 and 2.009 Å; C(Et)−Zn−C(Et), 132.16°).[17a] The Zn−N(amido) bond lengths in **10** (2.0825−2.0877 Å) and **11** (2.100(3) Å) are similar, indicating that the mononuclear unit in dimeric **10** has an equivalent effect as the $ZnEt_2$ fragment in **11**.

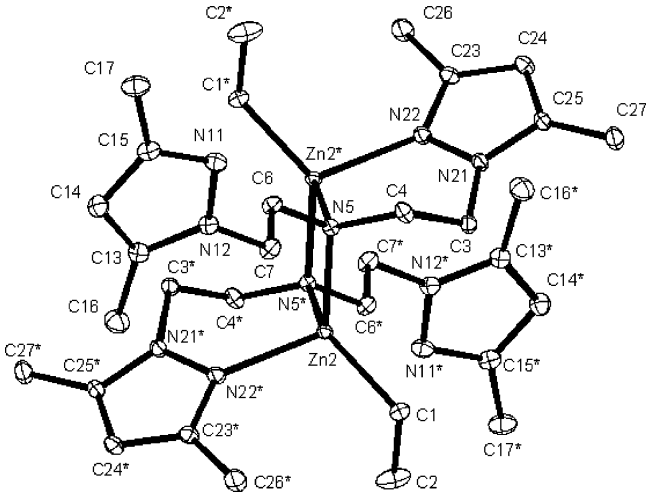

Figure 6. Solid-state structure of **10** (ellipsoids drawn at the 50% probability; hydrogen atoms omitted for clarity). Selected bond lengths (Å) and angles (deg): Zn(2)−C(1), 2.0124(12); Zn(2)−N(5), 2.0825(10); Zn(2)−N(5*), 2.0877(10); Zn(2)−N(22*), 2.1197(10); C(1)−Zn(2)−N(5), 122.48(5); C(1)−Zn(2)−N(22*), 109.65(5); C(1)−Zn(2)−N(5*), 124.63(5); N(22*)−Zn(2)−N(5*), 95.69(4); N(5)−Zn(2)−N(5*), 90.27(4); Zn(2)−N(5)−Zn(2*), 89.73(4).

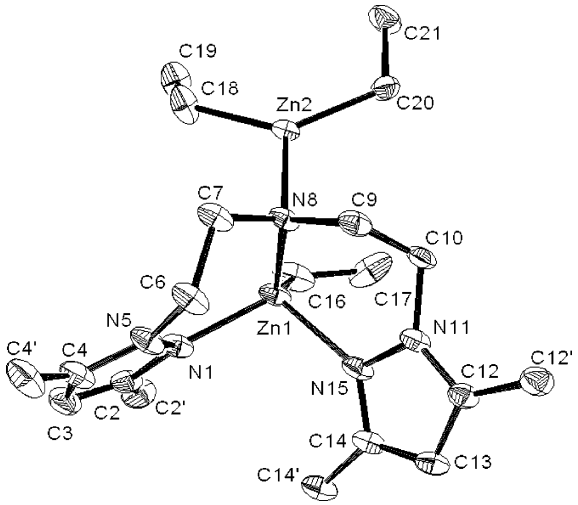

Figure 7. Solid-state structure of **11** (ellipsoids drawn at the 50% probability; hydrogen atoms omitted for clarity). Selected bond lengths (Å) and angles (deg): Zn(1)−C(16), 1.994(5); Zn(1)−N(15), 2.105(4); Zn(1)−N(1), 2.091(4); Zn(1)−N(8), 2.045(3); Zn(2)−N(8), 2.100(3); Zn(2)−C(18), 1.988(5); Zn(2)−C(20), 1.995(5); C(18)−Zn(2)−C(20), 137.0(2); C(16)−Zn(1)−N(1), 121.65(19); C(16)−Zn(1)−N(15), 107.7(2); N(1)−Zn(1)−N(15), 102.68(15); Zn(1)−N(8)−Zn(2), 93.73(13).

The two metal centers in the dinuclear mixed ethyl-ethoxide complex **12** are doubly bridged by the central N(amido) atom of the ligand and the O ethoxide atom, as observed in many zinc alkoxides (Figure 8). An approximate (noncrystallographic) symmetry axis goes through these two bridging atoms, provided one does not take into account the

(14) Andrews, P. C.; Raston, C. L.; Skelton, B. W.; White, A. H. *Organometallics* **1998**, *17*, 779−782; $ZnEt_2[Me_2NCH_2CH_2NMe_2]$, N−Zn−N, 80.68°, C−Zn−C, 118.08°.

(15) (a) Weng, S. *Main Group Met. Chem.* **1999**, *22*, 447−451; $ZnEt_2$-[substituted piperidine], N-Zn-N, 102.13°, C-Zn-C, 135.61°. (b) Wissing, E.; Havenith, R. W. A.; Boersma, J.; Smeets, W. J. J.; Spek, A. L.; van Koten, G. *J. Org. Chem.* **1993**, *58*, 4228−4236; $ZnEt_2$-[substituted pyridine], N−Zn−N, 89.41°, C−Zn−C, 145.75°.

(16) (a) Bell, N. A.; Moseley, P. T.; Shearer, H. M. M.; Spencer, C. B. *J. Chem. Soc., Chem. Commun.* **1980**, 359−360. (b) Bell, N. A.; Kassyk, A. L. *Inorg. Chim. Acta* **1996**, *250*, 345−349. (c) Malik, M. A.; O'Brien, P.; Motevalli, M.; Jones, A. C. *Inorg. Chem.* **1997**, *36*, 5076−5081. (d) Bette, V.; Mortreux, A.; Lehmann, C. W.; Carpentier, J.-F. *Chem. Commun.* **2003**, 332−333.

(17) (a) Arduengo, A. J., III; Dias, H. V. R.; Davidson, F.; Harlow, R. L. *J. Organomet. Chem.* **1993**, *462*, 13−18. (b) Boss, S. R.; Haigh, R.; Linton, D. J.; Schooler, P.; Shields, G. P.; Wheatley, A. E. H. *Dalton Trans.* **2003**, 1001−1008.

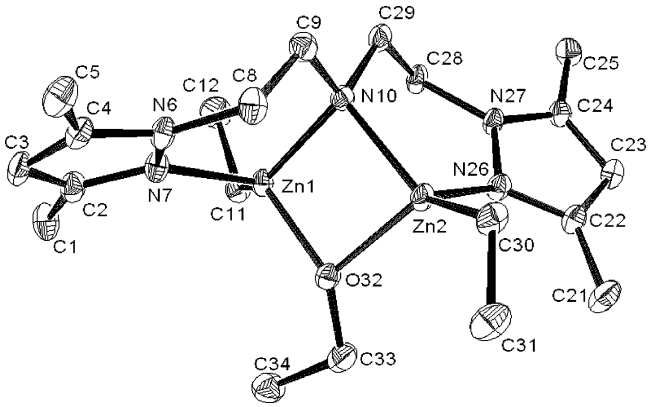

Figure 8. Solid-state structure of **12** (ellipsoids drawn at the 50% probability; hydrogen atoms omitted for clarity). Selected bond lengths (Å) and angles (deg): Zn(1)−C(11), 1.9954(19); Zn(1)−O(32), 2.0214(17); Zn(1)−N(10), 2.0732(17); Zn(1)−N(7), 2.1010(16); Zn(2)−N(10), 2.0595(18); Zn(2)−N(26), 2.1144(16); Zn(2)−O(32), 2.0087(15); Zn(2)−C(30), 1.9993(19); C(11)−Zn(1)−O(32), 122.08(7); C(11)−Zn(1)−N(7), 117.09(8); O(32)−Zn(1)−N(10), 86.08(6); Zn(1)−O(32)−Zn(2), 94.22(6); Zn(1)−N(10)−Zn(2), 91.20(6); N(10)−Zn(2)−O(32), 86.77(6).

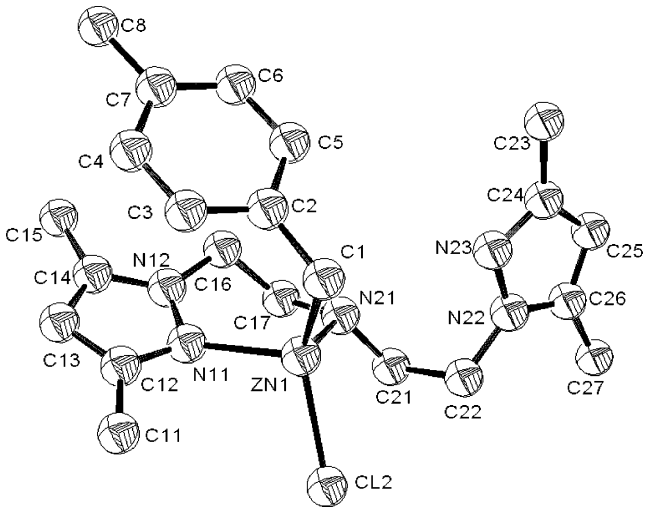

Figure 9. Solid-state structure of **14** (ellipsoids drawn at the 50% probability; hydrogen atoms omitted for clarity). Selected bond lengths (Å) and angles (deg): Zn(1)−C(1), 2.0182(17); Zn(1)−Cl(2), 2.2789(6); Zn(1)−N(11), 2.0876(14); Zn(1)−N(21), 2.1290(13); Cl(2)−Zn(1)−N(11), 106.71(4); Cl(2)−Zn(1)−N(21), 105.41(4); N(11)−Zn(1)−N(21), 92.55(5); C(1)−Zn(1)−Cl(2), 125.46(6); C(2)−C(1)−Zn(1), 107.35(11).

ethyl residue of the ethoxide ligand. The Zn−O and Zn−N(amido) bond lengths in **12** (Zn−O, 2.0214(17)−2.0087(15); Zn−N(10), 2.0595(18)−2.0732(17) Å) compare well with those observed in a mixed ethyl-oxide Zn complex of trimethylethylenediamine (Zn−O, 1.973−2.028; Zn−N 2.001−2.092 Å)[16b] and a tetranuclear ethyl-ethoxide Zn complex of tridentate pyridine ligands (Zn−O, 2.131−2.187; Zn−N, 2.144 Å).[18] The ZnOZnN metallacycle in **12** is slightly distorted from an ideal plane (torsion angle: 9.8°), as it is also in the two latter related compounds (torsion angles: 2.1 and 7.3°, respectively[16b,18]).

The solid-state structure of the benzyl-zinc chloride adduct **14** (Figure 9) is comparable to that of diethylzinc adduct **9**. The metal center is in a less distorted tetrahedral geometry with a larger N(pyrazolyl)−Zn−N(bridge) angle (N(11)−Zn(1)−N(21), 92.55(5)°) and a more acute C−Zn−Cl angle (C(1)−Zn(1)−Cl(2), 125.46(6)°). Both the Zn−N(pyrazolyl) (2.0876(14) Å) and Zn−N(bridge) (2.1290(13) Å) bond lengths are reduced as compared to those in **9** (2.214(3) and 2.263(3) Å, respectively), reflecting the electron-withdrawing effect of the chlorine ligand.

(18) Olmstead, M. M.; Grigsby, W. J.; Chacon, D. R.; Hascall, T.; Power, P. P. *Inorg. Chim. Acta* **1996**, *251*, 273−284.

Scheme 10

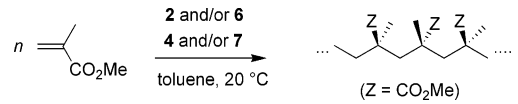

Table 3. MMA Polymerization Initiated by Aluminum Complexes[a]

entry	complex	Li-enolate (equiv)	yield (%)	*rr*[b] (%)	M_n[c] (g.mol^{-1})	M_w/M_n[c]
1	**2** or **4**		traces			
2	**2**	0.5	45	58	17 300	1.41
3	**2**	1.0	20	24	8300	1.26
4	**4**	0.5	40	29	15 500	1.36
5	**4**	1.0	25	31	9400	1.32
6	**8**		traces			
7[d]	**8**		8	58	50 900	3.97
8[d,e]	**8**		15	66	33 600	2.88

[a] Reaction time = 24 h (unoptimized), T = 20 °C, solvent = toluene (2.0 mL), [MMA]/[Al] = 200; cat. = 0.05 mmol, Li-enolate = LiO(*i*PrO)C=CMe$_2$. [b] Determined by ^{1}H NMR. [c] M_n and M_w/M_n values determined by GPC in THF vs polystyrene standards. [d] $B(C_6F_5)_3$ (1.0 equiv vs Al) was added. [e] (2,6-di-*t*Bu-4-Me−$C_6H_2O)_2$AlMe (1.0 equiv vs Al) was added.

MMA Polymerization Promoted by Aluminum Complexes. Methyl methacrylate (MMA) polymerization was investigated with the prepared aluminum complexes (Scheme 10). Representative results are given in Table 3. Neutral complexes **2**, **4**, and **8** are inactive toward MMA in toluene solution at 20 °C (entries 1 and 6). However, addition of the Li-ester enolate derived from isopropyl isobutyrate to **2** or **4**, to generate in situ the corresponding anionic aluminum species **6** and **7** (Schemes 2 and 3), leads to active systems. When 1 equiv of Li-ester enolate versus Al was used, poor conversions (20−25%) were observed from either **2** or **4** (entries 3 and 5). Higher conversions (40−45%) were observed upon adding only 0.5 equiv of Li-ester enolate versus Al (entries 2 and 4). These results evidence that the combination of an anionic Al species (i.e., **6** or **7**) as the initiator with a neutral Al species (**2** or **4**, respectively; left over because of the default of Li-ester enolate) generates a more effective system. This beneficial effect is assumed to arise from monomer activation by the Lewis acidic neutral species, as highlighted recently by Rodriguez-Delgado and Chen.[11] The systems generated under these conditions are not living but offer a certain degree of control as the PMMAs had relatively narrow polydispersities and experimental (uncorrected) number-average molecular weights slightly higher than the calculated values. Interestingly, only the system derived from **2** led to a significant syndiotacticity.

Poor results were observed with the enolate-aluminum complex **8** (entries 6−8). Addition of 1 equiv of the methyl abstractor $B(C_6F_5)_3$ to generate in situ cationic Al-enolate species (entry 7), further combined with 1 equiv of the bulky aluminum Lewis acid $(BHT)_2$AlMe ((2,6-di-*t*Bu-4-Me-

Scheme 11

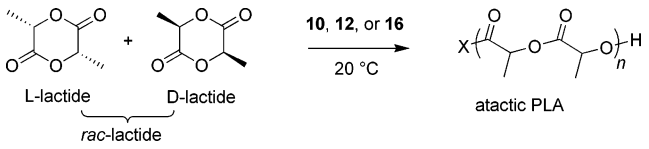

$C_6H_2O)_2AlMe$, also-called MAD)[11] (entry 8), improved MMA conversions. However, the initiation efficiency remained low (ca. 5−10%), and the molecular weight distributions of the PMMAs, though monodisperse, were broad.

***rac*-Lactide Polymerization Initiated by Zinc Complexes.** Zinc complexes **10**, **12**, and **16** were assessed in the polymerization of *rac*-lactide (Scheme 11).[19] Representative results are summarized in Table 4. All three complexes proved significantly active, allowing conversions of 100−400 equiv of *rac*-lactide at room temperature. For instance, polymerization initiated by **12** in dichloromethane at 20 °C proceeded with turnover frequencies of ca. 60 h^{-1} (Figure 10). In terms of degree of control of the polymerizations, the ethoxide dinuclear complex **12** proved a much better initiator than the ethyl-amido complex **10** and its cationic derivative **16**. As a matter of fact, the PLAs (polylactides) produced with **12** had a relatively narrow molecular weight distribution (M_w/M_n = 1.23−1.40), and the experimental (uncorrected) number-average molecular weights are in close agreement with the calculated values. Also, the M_n values of the PLAs increased linearly with the [LA]/[**12**] ratio (Figure 11). These results are consistent with a controlled-living polymerization model. On the other hand, the PLAs produced by **10** and **16** had broader polydispersities (M_w/M_n = 1.71−1.97) and either lower or larger M_n values (entries 9 and 17). Two possibilities can account for the relatively broad polydispersities observed with complex **10**: (1) because of the use as initiator of a Zn-alkyl(ethyl) group, which is known to be less nucleophilic than alkoxides (i.e., ethoxide in **12**), initiation is delayed versus propagation[19] and (2) backbiting reaction/transesterification takes place as side reactions, resulting in the formation of macrocycles with a wide range of molecular weight distribution. The lower M_n values (as compared to those expected for a well-controlled polymerization) observed with **10** are also diagnostic of transfer reactions. These results highlight the importance of differences in the coordination sphere between the mononuclear complex **10** and the dinuclear complex **12** on their polymerization performance. On the other hand, the significantly poorer control featured by cationic complex **16** in lactide polymerization, in particular its low initiation efficiency, as compared to **12** and even **10**, arguably call for fundamental mechanistic differences.[20] The homo-decoupled ^{1}H NMR spectra of the methine regions of PLAs, both produced in THF and toluene by **12**, show an atactic microstructure.

Experimental Section

General Procedures. All experiments were carried out under purified argon using standard Schlenk techniques or in a glovebox (<1 ppm O_2, 5 ppm H_2O). Hydrocarbon solvents, diethyl ether, and tetrahydrofuran were distilled from Na/benzophenone, and toluene and pentane were distilled from Na/K alloy under nitrogen and were degassed by freeze−thaw−vacuum cycles prior to use. Chlorinated solvents were distilled from calcium hydride. Deuterated solvents were purchased from Eurisotop and were purified before use. Methyl methacrylate (MMA, Acros) was distilled twice under argon over CaH_2. *rac*-Lactide (Aldrich) was sublimed twice before use. 3,5-Dimethylpyrazole, bis(2-chloroethyl)-amine hydrochloride, 2,4,6-trimethylacetophenone, NaH, $AlMe_3$, $AlEt_3$, $ZnEt_2$, and $ZnCH_2C_6H_4$-*p*-CH_3(Cl) (all Aldrich) and $ZnCl_2$ (Acros) were used as received. $B(C_6F_5)_3$ (Boulder Scientific Co.) was sublimed twice before use.

NMR spectra were recorded on Bruker AC-200, AC-300, and AM-500 spectrometers in Teflon-valved NMR tubes at 23 °C unless otherwise stated. ^{1}H and ^{13}C NMR chemical shifts were determined using residual solvent resonances and are reported versus $SiMe_4$. Assignment of signals was made from ^{1}H−^{13}C HMQC and ^{1}H−^{13}C HMBC 2D NMR experiments. Coupling constants are given in hertz. Elemental analyses (C, H, N) were performed by the Microanalytical Laboratory at the Institute of Chemistry of Rennes and are the average of two independent determinations. Molecular weights of PMMA (or PLA) were determined by gel permeation chromatography (GPC) at room temperature on a Waters apparatus equipped with five PL gel columns (Polymer Laboratories Ltd), an autosampler Waters WISP 717, and a differential refractometer Shimadzu RID 6A. THF was used as eluent at a flow rate of 1.0 mL.min^{-1}. Polystyrene standards were used for molecular weight universal calibration. The microstructure of polymers was determined by ^{1}H NMR in $CDCl_3$.

Bis[2-(3,5-dimethyl-1-pyrazolyl)ethyl]amine (1). A modified method[21] was used to synthesize ligand **1**. To a 100-mL Schlenk containing a suspension of NaH (1.38 g, 57.4 mmol) in DMF (50 mL) was added dropwise a solution of 3,5-dimethylpyrazole (3.68 g, 38.3 mmol) in DMF (10 mL). The reaction mixture was stirred for 2 h at room temperature. Then, a solution of bis(2-chloroethyl)-amine hydrochloride (3.41 g, 19.1 mmol) in DMF (10 mL) was added dropwise to the mixture. The reaction mixture was further stirred for 2 h at 70 °C, yielding a cream white dispersion which was cooled and filtered. The filtrate was evaporated to dryness in vacuo, and then hot water (80 °C, 10 mL) was added. Cooling gave white needle crystals of **1** (3.24 g, 65%). ^{1}H NMR ($CDCl_3$): δ 5.74 (s, 2H, pyrazole-*H*), 4.01 (t, ^3J = 6.0, 4H, NCH_2CH_2-pyrazole), 2.95 (t, ^3J = 6.0, 4H, NCH_2CH_2-pyrazole), 2.19 (s, 6H, pyrazole-CH_3), 2.16 (s, 6H, pyrazole-CH_3). ^{1}H NMR (C_6D_6): δ 5.69 (s, 2H, pyrazole-*H*), 3.61 (t, ^3J = 6.0, 4H, NCH_2CH_2-pyrazole), 2.70 (t, ^3J

(19) For lactide polymerization initiated by discrete Zn-alkoxide complexes, see: (a) Cheng, M.; Attygalle, A. B.; Lobkovsky, E. B.; Coates, G. W. *J. Am. Chem. Soc.* **1999**, *121*, 11583−11584. (b) Chamberlain, B. M.; Cheng, M.; Moore, D. R.; Ovitt, T. M.; Lobkovsky, E. B.; Coates, G. W. *J. Am. Chem. Soc.* **2001**, *123*, 3229−3238. (c) Chisholm, M. H.; Gallucci, J. C.; Zhen, H.; Huffman, J. C. *Inorg. Chem.* **2001**, *40*, 5051−5054. (d) Chisholm, M. H.; Huffman, J. C.; Phomphrai, K. *Dalton Trans.* **2001**, 222−224. (e) Williams, C. K.; Breyfogle, L. E.; Choi, S. K.; Nam, W.; Young, V. G., Jr.; Hillmyer, M. A.; Tolman, W. B. *J. Am. Chem. Soc.* **2003**, *125*, 11350−11359. (f) Jensen, T. R.; Schaller, C. P.; Hillmyer, M. A.; Tolman, W. B. *J. Organomet. Chem.* **2005**, *690*, 5881−5891. (g) Chisholm, M. H.; Gallucci, J. C.; Phomphrai, K. *Inorg. Chem.* **2005**, *44*, 8004−8010. (h) Chen, H.-Y.; Tang, H.-Y.; Lin, C.-C. *Macromolecules* **2006**, *39*; 3745−3752.

(20) Contrary to polymerizations of *rac*-lactide carried out with **10** and **12**, which likely proceed via a coordination-insertion mechanism, those with **16** are assumed to occur via a cationic mechanism, though this was not established in the present case.

(21) Martens, C. F.; Schenning, A. P. H. J.; Feiters, M. C.; Berens, H. W.; van der Linden, J. G. M.; Admiraal, G.; Beurskens, P. T.; Kooijman, H.; Spek, A. L.; Nolte, R. J. M. *Inorg. Chem.* **1995**, *34*, 4735−4744.

Table 4. *rac*-Lactide Polymerization Initiated by Complexes **10**, **12**, and **16**[a]

entry	complex	[LA]/[complex]	solvent	conv. (%)	$M_{n,calc}$[b] (g.mol^{-1})	$M_{n,exp}$[c] (g.mol^{-1})	M_w/M_n[c]
9	**10**	100	THF	93	13 400	8500	1.71
10	**12**	100	THF	95	13 700	14 400	1.23
11	**12**	100	toluene	98	14 100	12 500	1.32
12	**12**	200	toluene	93	26 800	22 700	1.30
13	**12**	100	CH_2Cl_2	>99	14 400	14 700	1.34
14	**12**	200	CH_2Cl_2	>99	28 900	22 500	1.29
15	**12**	300	CH_2Cl_2	>99	43 300	29 500	1.38
16	**12**	400	CH_2Cl_2	>99	57 700	38 500	1.40
17	**16**	100	CH_2Cl_2	98	14 100	111 000	1.97

[a] Reaction time = 30 h (unoptimized), T = 20 °C, solvent = 2.5 mL, complex = 0.01 mmol. [b] Calculated $M_{n,calc}$ values considering one polymer chain per initiator. [c] Experimental M_n and M_w/M_n values determined by GPC in THF vs PS standards.

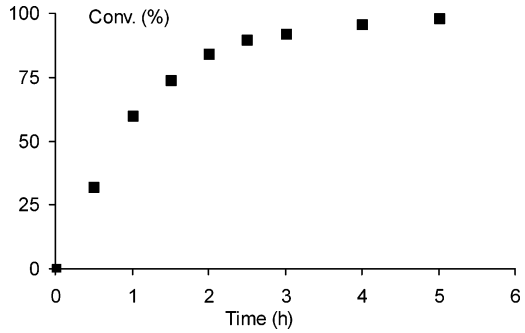

Figure 10. Kinetics of *rac*-lactide conversion with ethoxide zinc complex **12** (for polymerization conditions, see Table 4, entry 13).

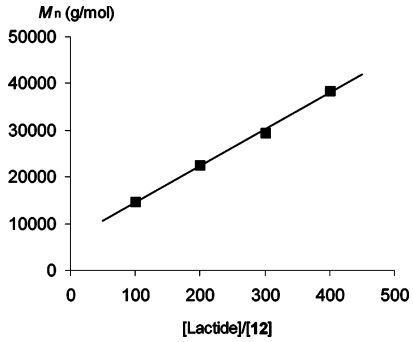

Figure 11. Variation of the number-average molecular weights of PLAs as a function of monomer-to-initiator ratio (for polymerization conditions, see Table 4, entries 13−16).

= 6.0, 4H, NCH_2CH$_2$-pyrazole), 2.29 (s, 6H, pyrazole-CH_3), 1.81 (s, 6H, pyrazole-CH_3).

Bis[2-(3,5-dimethyl-1-pyrazolyl)ethylamine]AlMe$_3$ (2). To a 50-mL Schlenk containing $AlMe_3$ (0.38 mL of a 2.0 M solution, 0.76 mmol) in pentane (2 mL) was added dropwise bis[2-(3,5-dimethyl-1-pyrazolyl)ethyl]amine (0.20 g, 0.76 mmol) in toluene (5 mL). The mixture was stirred for 6 h at room temperature. The solvent was removed under vacuum, leaving a colorless oil that was recrystallized with pentane to give block colorless crystals of **2** (0.22 g, 87%). A suitable crystal was selected for X-ray diffraction analysis. ^{1}H NMR (C_6D_6): δ 5.53 (s, 2H, pyrazole-*H*), 3.56 (m, 4H, NCH$_2$CH_2-pyrazole), 2.80 (m, 4H, NCH_2CH$_2$-pyrazole), 2.12 (s, 6H, pyrazole-CH_3), 1.71 (s, 6H, pyrazole-CH_3), −0.39 (s, 9H, Al(CH_3)$_3$). ^{1}H NMR (Tol-d_8): δ 5.54 (s, 2H, pyrazole-*H*), 4.57 (br s, 1H, N*H*), 3.60 (m, 4H, NCH$_2$CH_2-pyrazole), 2.85 (m, 4H, NCH_2-CH$_2$-pyrazole), 2.13 (s, 6H, pyrazole-CH_3), 1.80 (s, 6H, pyrazole-CH_3), −0.46 (s, 9H, Al(CH_3)$_3$). ^{1}H NMR (CD_2Cl_2): δ 5.80 (s, 2H, pyrazole-*H*), 4.10 (m, 4H, NCH$_2$CH_2-pyrazole), 3.17 (m, 4H, NCH_2-CH$_2$-pyrazole), 2.24 (s, 6H, pyrazole-CH_3), 2.16 (s, 6H, pyrazole-CH_3), −0.90 (s, 9H, Al(CH_3)$_3$). ^{1}H NMR (THF-d_8): 5.65 (s, 2H, pyrazole-*H*), 3.94 (t, ^3J = 6.1, 4H, NCH$_2$CH_2-pyrazole), 2.90 (t, ^3J = 6.1, 4H, NCH_2CH$_2$-pyrazole), 2.16 (s, 6H, pyrazole-CH_3), 2.06 (s, 6H, pyrazole-CH_3), −0.97 (s, 9H, Al(CH_3)$_3$). ^{13}C{^{1}H} NMR (C_6D_6): δ 147.62 (pyrazole-*C*CH$_3$), 138.71 (pyrazole-*C*CH$_3$), 105.00 (pyrazole-*C*H), 47.84 (NCH$_2$CH$_2$-pyrazole), 44.52 (NCH$_2$*C*H$_2$-pyrazole), 13.39 (pyrazole-*C*H$_3$), 10.29 (pyrazole-*C*H$_3$), −8.33 (Al-(*C*H$_3$)$_3$). Anal. calcd. for $C_{17}H_{32}AlN_5$ (333.45): C, 61.23; H, 9.67; N, 21.00; found: C, 60.72; H, 9.34; N, 21.50.

Bis[2-(3,5-dimethyl-1-pyrazolyl)ethylamine]AlEt$_3$ (3). The same procedure was used as that described for **2**, starting from $AlEt_3$ (1.45 mL of a 1.9 M solution, 2.75 mmol) and bis[2-(3,5-dimethyl-1-pyrazolyl)ethyl]amine (0.72 g, 2.75 mmol), yielding block colorless crystals of **3** (0.85 g, 82%). ^{1}H NMR (C_6D_6): δ 5.54 (s, 2H, pyrazole-*H*), 5.11 (s br, 1H, N*H*), 3.56 (m, 4H, NCH$_2$CH_2-pyrazole), 2.72 (m, 4H, NCH_2CH$_2$-pyrazole), 2.12 (s, 6H, pyrazole-CH_3), 1.71 (s, 6H, pyrazole-CH_3), 1.45 (t, ^3J = 8.1, 9H, AlCH$_2$CH_3), 0.21 (q, ^3J = 8.1, 6H, AlCH_2CH$_3$). ^{13}C{^{1}H} NMR (C_6D_6): δ 147.62 (pyrazole-*C*CH$_3$), 138.71 (pyrazole-*C*CH$_3$), 105.30 (pyrazole-*C*H), 47.48 (NCH$_2$CH$_2$-pyrazole), 43.98 (NCH$_2$*C*H$_2$-pyrazole), 13.45 (pyrazole-*C*H$_3$), 10.22 (pyrazole-*C*H$_3$), 10.09 (AlCH$_2$*C*H$_3$), −0.29 (Al*C*H$_2$CH$_3$). Anal. calcd. for $C_{20}H_{38}AlN_5$ (375.53): C, 63.97; H, 10.20; N, 18.65; found: C, 62.90; H, 10.15; N, 18.92.

[Bis[2-(3,5-dimethyl-1-pyrazolyl)ethyl]amide]AlMe$_2$ (4). In the glovebox, a Teflon-valved NMR tube was charged with **2** (50.0 mg, 0.15 mmol), and C_6D_6 (ca. 0.5 mL) or toluene-d_8 (ca. 0.5 mL) was vacuum transferred in. The tube was sealed and kept at 80 °C for 24 h. NMR spectroscopy was recorded, which revealed quantitative formation of **4**, together with release of CH_4 (δ ^{1}H (C_6D_6) 0.15 ppm, δ ^{1}H (toluene-d_8) 0.22 ppm). The solution was dried in vacuo, and the white solid residue was recrystallized from pentane at −34 °C to give colorless crystals of **4** (42 mg, 88%). A suitable crystal was selected for X-ray diffraction analysis. ^{1}H NMR (C_6D_6): δ 5.48 (s, 2H, pyrazole-*H*), 3.62 (t, ^3J = 6.1, 4H, NCH$_2$CH_2-pyrazole), 3.20 (t, ^3J = 6.1, 4H, NCH_2CH$_2$-pyrazole), 2.21 (s, 6H, pyrazole-CH_3), 1.68 (s, 6H, pyrazole-CH_3), −0.31 (s, 6H, Al(CH_3)$_2$). ^{1}H NMR (Tol-d_8): δ 5.52 (s, 2H, pyrazole-*H*), 3.65 (t, ^3J = 5.5, 4H, NCH$_2$CH_2-pyrazole), 3.19 (t, ^3J = 5.5, 4H, NCH_2-CH$_2$-pyrazole), 2.23 (s, 6H, pyrazole-CH_3), 1.77 (s, 6H, pyrazole-CH_3), −0.38 (s, 6H, Al(CH_3)$_2$). ^{1}H NMR (toluene-d_8, 0 °C): δ 5.50 (s, 1H, pyrazole-*H*), 5.49 (s, 1H, pyrazole-*H*), 3.63 (s, 2H, NCH$_2$CH_2-pyrazole), 3.62 (s, 2H, NCH$_2$CH_2-pyrazole), 3.20 (s, 2H, NCH_2CH$_2$-pyrazole), 3.19 (s, 2H, NCH_2CH$_2$-pyrazole), 2.25 (s, 3H, pyrazole-CH_3), 2.24 (s, 3H, pyrazole-CH_3), 1.75 (s, 3H, pyrazole-CH_3), 1.74 (s, 3H, pyrazole-CH_3), −0.33 (s, 3H, Al(CH_3)$_2$), −0.34 (s, 3H, Al(CH_3)$_2$). ^{13}C{^{1}H} NMR (toluene-d_8): δ 147.03 (pyrazole-*C*CH$_3$), 139.79 (pyrazole-*C*CH$_3$), 104.91 (pyrazole-*C*H), 51.03 (NCH$_2$CH$_2$-pyrazole), 49.74 (NCH$_2$*C*H$_2$-pyrazole), 12.98 (pyrazole-*C*H$_3$), 10.22 (pyrazole-*C*H$_3$), −8.51 (Al(*C*H$_3$)$_2$). Anal. calcd. for $C_{16}H_{28}AlN_5$ (317.41): C, 60.54; H, 8.89; N, 22.06; found: C, 60.92; H, 8.78; N, 22.35.

[Bis[2-(3,5-dimethyl-1-pyrazolyl)ethyl]amide]AlEt$_2$ (5). The same procedure was used as for **4**, starting from **3** (50.0 mg, 0.130 mmol), giving complex **5** over 95% NMR purity. ^{1}H NMR (C_6D_6): δ 5.50 (s, 2H, pyrazole-*H*), 3.67 (t, ^3J = 6.1, 4H, NCH$_2$C*H*$_2$-pyrazole), 3.24 (t, ^3J = 6.1, 4H, NC*H*$_2$CH$_2$-pyrazole), 2.34 (s, 6H, pyrazole-C*H*$_3$), 1.69 (s, 6H, pyrazole-C*H*$_3$), 1.38 (t, ^3J = 8.1, 6H, AlCH$_2$C*H*$_3$), 0.33 (q, ^3J = 8.1, 4H, AlC*H*$_2$CH$_3$). ^{13}C{^{1}H} NMR (C_6D_6): δ 147.55 (pyrazole-*C*CH$_3$), 140.26 (pyrazole-*C*CH$_3$), 105.41 (pyrazole-*C*H), 51.63 (N*C*H$_2$CH$_2$-pyrazole), 50.23 (NCH$_2$*C*H$_2$-pyrazole), 13.14 (pyrazole-*C*H$_3$), 10.68 (pyrazole-*C*H$_3$), 10.16 (AlCH$_2$*C*H$_3$), 1.37 (Al*C*H$_2$CH$_3$). Anal. calcd. for $C_{18}H_{32}AlN_5$ (345.46): C, 62.58; H, 9.34; N, 20.27; found: C, 61.85; H, 9.67; N, 20.78.

Reaction of 2 with LiO(*i*PrO)C═CMe$_2$: Generation of 6. In the glovebox, complex **2** (21.6 mg, 0.065 mmol) and LiO(*i*PrO)C═CMe$_2$ (8.8 mg, 0.065 mmol) were charged in a Teflon-valved NMR tube, and C_6D_6 (ca. 0.5 mL) was vacuum transferred in. ^{1}H NMR spectroscopy was recorded, which revealed the quantitative formation of **6**, together with release of 1 equiv of (CH$_3$)$_2$CHCO$_2$*i*Pr. The solution was dried in vacuo, and the white solid residue was recrystallized from pentane at −34 °C to give colorless crystals of **6** (17 mg, 75%), of which some were suitable for X-ray diffraction analysis. ^{1}H NMR (C_6D_6): δ 5.53 (s, 2H, pyrazole-*H*), 3.72 (m, 2H, NCH$_2$C*H*$_2$-pyrazole, syn), 3.58 (m, 2H, NC*H*$_2$CH$_2$-pyrazole, syn), 3.49 (m, 2H, NCH$_2$C*H*$_2$-pyrazole, anti), 2.53 (m, 2H, NC*H*$_2$-CH$_2$-pyrazole, anti), 2.09 (s, 6H, pyrazole-C*H*$_3$), 1.59 (s, 6H, pyrazole-C*H*$_3$), −0.39 (s, 9H, Al(C*H*$_3$)$_3$). ^{13}C{^{1}H} NMR (C_6D_6): δ 147.56 (pyrazole-*C*CH$_3$), 139.72 (pyrazole-*C*CH$_3$), 104.63 (pyrazole-*C*H), 54.43 (N*C*H$_2$CH$_2$-pyrazole), 49.06 (NCH$_2$*C*H$_2$-pyrazole), 13.06 (pyrazole-*C*H$_3$), 10.43 (pyrazole-*C*H$_3$), −8.10 (Al(*C*H$_3$)$_3$). NMR data for (CH$_3$)$_2$CHCO$_2$*i*Pr: ^{1}H NMR (C_6D_6): δ 5.01 (sept, ^3J = 6.9, 1H, OC*H*(CH$_3$)$_2$), 2.36 (sept, ^3J = 6.3, 1H, (CH$_3$)$_2$C*H*CO), 1.05 (d, ^3J = 6.9, 6H, OCH(C*H*$_3$)$_2$), 1.02 (d, ^3J = 6.3, 6H, (C*H*$_3$)$_2$-CHCO). ^{13}C{^{1}H} NMR (C_6D_6): δ 176.51 (*C*O*i*Pr), 67.02 (O*C*H-(CH$_3$)$_2$), 34.43 ((CH$_3$)$_2$*C*HCO), 21.49 (OCH(*C*H$_3$)$_2$), 18.87 ((*C*H$_3$)$_2$-CHCO). Anal. calcd. for $C_{17}H_{31}AlLiN_5$ (339.38): C, 60.16; H, 9.21; N, 20.64; found: C, 60.32; H, 9.18; N, 20.75.

Reaction of 4 with LiO(*i*PrO)C═CMe$_2$: Generation of 7. Complex **4** (30.0 mg, 0.090 mmol) and LiO(*i*PrO)C═CMe$_2$ (12.2 mg, 0.090 mmol) were charged in a Teflon-valved NMR tube, and C_6D_6 (ca. 0.5 mL) was vacuum transferred in. ^{1}H NMR spectroscopy was recorded, which revealed the quantitative formation of **7**. ^{1}H NMR (C_6D_6): δ 5.54 (s, 2H, pyrazole-*H*), 4.54 (sept, ^3J = 6.2, 1H, OC*H*(CH$_3$)$_2$), 3.63 (m, 2H, NCH$_2$C*H*$_2$-pyrazole, syn), 3.55 (m, 2H, NC*H*$_2$CH$_2$-pyrazole, syn), 3.33 (m, 2H, NCH$_2$C*H*$_2$-pyrazole, anti), 2.48 (m, 2H, NC*H*$_2$CH$_2$-pyrazole, anti), 2.18 (s, 6H, pyrazole-C*H*$_3$), 1.94 (s, 3H, (C*H*$_3$)$_2$C═C), 1.84 (s, 3H, (C*H*$_3$)$_2$C═C), 1.59 (s, 6H, pyrazole-C*H*$_3$), 1.27 (d, ^3J = 6.2, 6H, OCH(C*H*$_3$)$_2$), −0.34 (s, 6H, Al(C*H*$_3$)$_2$). ^{13}C{^{1}H} NMR (C_6D_6): δ 150.59 ((CH$_3$)$_2$C═*C*), 147.60 (pyrazole-*C*CH$_3$), 139.06 (pyrazole-*C*CH$_3$), 104.85 (pyrazole-*C*H), 84.78 ((CH$_3$)$_2$*C*═C), 68.01 ((CH$_3$)$_2$*C*HO), 54.43 (N*C*H$_2$CH$_2$-pyrazole), 49.69 (NCH$_2$*C*H$_2$-pyrazole), 22.25 ((*C*H$_3$)$_2$-CHO), 18.02 ((*C*H$_3$)$_2$C═C), 13.11 (pyrazole-*C*H$_3$), 10.45 (pyrazole-*C*H$_3$), −8.90 (Al(*C*H$_3$)$_2$).

Reaction of 4 with 2,4,6-Trimethylacetophenone: Generation of 8. Complex **4** (11.5 mg, 0.036 mmol) and 2,4,6-Me$_3$C$_6$H$_2$COCH$_3$ (5.8 mg, 0.036 mmol) were charged in a Teflon-valved NMR tube, and C_6D_6 (ca. 0.5 mL) was vacuum transferred in. ^{1}H NMR spectroscopy was recorded, which revealed the quantitative formation of **8** within 2 h. ^{1}H NMR (C_6D_6): δ 6.68 (s, 2H, Ph), 5.67 (s, 2H, pyrazole-*H*), 4.79 (d, ^2J = 2.4, 1H, C═CH*H*), 4.03 (d, ^2J = 2.4, 1H, C═C*H*H), 3.61 (t, ^3J = 6.0, 4H, NCH$_2$C*H*$_2$-pyrazole), 2.71 (q, ^3J = 6.0, 4H, NC*H*$_2$CH$_2$-pyrazole), 2.32 (s, 6H, *o*-C*H*$_3$-Ph), 2.26 (s, 6H, pyrazole-C*H*$_3$), 2.00 (s, 3H, *p*-C*H*$_3$-Ph), 1.80 (s, 6H, pyrazole-C*H*$_3$), −0.52 (s, 6H, Al(C*H*$_3$)$_2$). ^{13}C{^{1}H} NMR (C_6D_6): δ 153.22 (O*C*═CH$_2$), 147.54 (pyrazole-*C*CH$_3$), 138.73 (Ph), 138.38 (pyrazole-*C*CH$_3$), 136.82 (Ph), 132.75 (Ph), 128.33 (Ph), 104.50 (pyrazole-*C*H), 95.54 (C═*C*H$_2$), 49.14 (N*C*H$_2$CH$_2$-pyrazole), 47.90 (NCH$_2$*C*H$_2$-pyrazole), 20.78 (*p*-*C*H$_3$-Ph), 20.05 (*o*-*C*H$_3$-Ph), 13.60 (pyrazole-*C*H$_3$), 10.57 (pyrazole-*C*H$_3$), −9.89 (Al(*C*H$_3$)$_2$).

Reaction of 2 with 2,4,6-Trimethylacetophenone: Generation of 8. Complex **2** (12.0 mg, 0.036 mmol) and 2,4,6-Me$_3$C$_6$H$_2$COCH$_3$ (5.8 mg, 0.036 mmol) were charged in a Teflon-valved NMR tube, and C_6D_6 (ca. 0.5 mL) was vacuum transferred in. ^{1}H NMR spectroscopy was recorded, which revealed the formation of **8** (>95%) within 6 h at 60 °C. The NMR data of complex **8** were the same as those reported above.

[Bis[2-(3,5-dimethyl-1-pyrazolyl)ethyl]amine]ZnEt$_2$ (9). To a solution of ligand **1** (0.306 g, 1.17 mmol) in toluene (5 mL) was slowly added ZnEt$_2$ (1.01 g, 15 wt % solution in hexane, 1.23 mmol) at room temperature. The reaction mixture was stirred for 2 h. After evaporation of volatiles under vacuum, the residue was recrystallized from a ca. 1:10 toluene/pentane solution at −34 °C to give colorless crystals of **9** (0.406 g, 90%). A suitable crystal was selected for X-ray diffraction analysis. ^{1}H NMR (C_6D_6): δ 5.61 (s, 2H, pyrazole-*H*), 3.52 (t, ^3J = 5.5, 4H, NCH$_2$C*H*$_2$-pyrazole), 2.68 (q, ^3J = 5.5, 4H, NC*H*$_2$CH$_2$-pyrazole), 2.29 (s, 6H, pyrazole-C*H*$_3$), 1.70 (s, 6H, pyrazole-C*H*$_3$), 1.55 (t, ^3J = 8.1, 6H, Zn(CH$_2$C*H*$_3$)$_2$), 0.42 (q, ^3J = 8.1, 4H, Zn(C*H*$_2$CH$_3$)$_2$). ^{13}C{^{1}H} NMR (C_6D_6): δ 147.64 (pyrazole-*C*CH$_3$), 138.78 (pyrazole-*C*CH$_3$), 104.89 (pyrazole-*C*H), 49.11 (N*C*H$_2$CH$_2$-pyrazole), 46.61 (NCH$_2$*C*H$_2$-pyrazole), 13.99 (Zn(CH$_2$*C*H$_3$)$_2$), 13.47 (pyrazole-*C*H$_3$), 10.45 (pyrazole-*C*H$_3$), 2.83 (Zn(*C*H$_2$CH$_3$)$_2$). Anal. calcd. for $C_{18}H_{33}N_5Zn$ (384.88): C, 56.17; H, 8.64; N, 18.20; found: C, 55.83; H, 8.32; N, 18.65.

[Bis[2-(3,5-dimethyl-1-pyrazolyl)ethyl]amide]ZnEt (10). In the glovebox, complex **9** (0.105 g, 0.273 mmol) was charged in a Teflon-valved NMR tube, and C_6D_6 (ca. 0.5 mL) was vacuum transferred in. The tube was sealed and kept at 60 °C for 2 days. ^{1}H NMR spectroscopy was recorded, which revealed the quantitative formation of **10**, together with release of CH$_3$CH$_3$ (δ ^{1}H (C_6D_6) 0.79 ppm). Cooling the solution gave large amounts of colorless crystals of **10** (92 mg, 94%), of which some were suitable for X-ray diffraction analysis. ^{1}H NMR (C_6D_6): δ 5.58 (s, 2H, pyrazole-*H*), 4.05 (t, ^3J = 6.0, 4H, NCH$_2$C*H*$_2$-pyrazole), 3.30 (t, ^3J = 6.0, 4H, NC*H*$_2$CH$_2$-pyrazole), 2.25 (s, 6H, pyrazole-C*H*$_3$), 1.75 (s, 6H, pyrazole-C*H*$_3$), 1.54 (t, ^3J = 8.0, 3H, ZnCH$_2$C*H*$_3$), 0.55 (q, ^3J = 8.0, 4H, ZnC*H*$_2$CH$_3$). ^{13}C{^{1}H} NMR (C_6D_6): δ 147.47 (pyrazole-*C*CH$_3$), 139.03 (pyrazole-*C*CH$_3$), 104.87 (pyrazole-*C*H), 54.47 (N*C*H$_2$CH$_2$-pyrazole), 47.91 (NCH$_2$*C*H$_2$-pyrazole), 14.35 (ZnCH$_2$*C*H$_3$), 13.46 (pyrazole-*C*H$_3$), 10.56 (pyrazole-*C*H$_3$), 1.10 (ZnC*H*$_2$CH$_3$). Anal. calcd. for $C_{16}H_{27}N_5Zn$ (354.81): C, 54.16; H, 7.67; N, 19.74; found: C, 54.05; H, 7.48; N, 19.86.

[Bis[2-(3,5-dimethyl-1-pyrazolyl)ethyl]amide]ZnEt.ZnEt$_2$ (11). To a solution of **1** (128 mg, 0.49 mmol) in toluene (5 mL) was slowly added ZnEt$_2$ (1.33 mL of a 1.1 M solution in toluene, 1.46 mmol) at room temperature. The reaction mixture was stirred for 16 h at 120 °C under strictly anaerobic conditions. Volatiles were removed under vacuum, and the solid residue was analyzed by ^{1}H NMR in C_6D_6, revealing the formation of **10** (ca. 80%) with other multiple, complex resonances assigned to the diethylzinc adduct (**11**; ca. 20%). The residue was recrystallized from toluene at −34 °C to give a few colorless crystals of **11**, which proved suitable for X-ray diffraction analysis.

[Bis[2-(3,5-dimethyl-1-pyrazolyl)ethyl]amide]Zn$_2$Et$_2$(μ-OEt) (12). (a) Synthesis of 12 from ZnEt$_2$ and 1 under Aerobic

Conditions. The reaction was carried out as described above, starting from commercial (unpurified) $ZnEt_2$ (1.33 mL of a 1.1 M solution in toluene, 1.46 mmol), ligand **1** (128 mg, 0.49 mmol), and carrying out the reaction without special care (i.e., traces of O_2 were present). Recrystallization of the final solid residue from toluene at −34 °C gave colorless crystals of **12** (88 mg, 36%), some of which proved suitable for X-ray diffraction analysis. ^{1}H NMR (C_6D_6): δ 5.46 (s, 2H, pyrazole-*H*), 4.27 (q, ^3J = 6.9, 2H, OCH_2CH_3), 4.11 (m, 4H, NCH_2CH_2-pyrazole), 3.05 (m, 4H, NCH_2-CH_2-pyrazole), 2.35 (s, 6H, pyrazole-CH_3), 1.71 (t, ^3J = 8.1, 6H, $ZnCH_2CH_3$), 1.52 (s, 6H, pyrazole-CH_3), 1.47 (t, ^3J = 6.9, 3H, OCH_2CH_3), 0.67 (q, ^3J = 8.1, 4H, $ZnCH_2CH_3$). ^{1}H NMR (CD_2Cl_2): δ 5.94 (s, 2H, pyrazole-*H*), 4.34 (m, 4H, NCH_2CH_2-pyrazole), 3.76 (q, ^3J = 6.8, 2H, OCH_2CH_3), 3.18 (m, 4H, NCH_2CH_2-pyrazole), 2.35 (s, 6H, pyrazole-CH_3), 2.29 (s, 6H, pyrazole-CH_3), 1.13 (t, ^3J = 8.1, 6H, $ZnCH_2CH_3$), 1.09 (t, ^3J = 6.9, 3H, OCH_2CH_3), 0.01 (q, ^3J = 8.1, 4H, $ZnCH_2CH_3$). ^{13}C{^{1}H} NMR (C_6D_6): δ 148.64 (pyrazole-CCH_3), 139.86 (pyrazole-CCH_3), 105.24 (pyrazole-*C*H), 61.89 (OCH_2CH_3), 57.04 (NCH_2CH_2-pyrazole), 48.56 (NCH_2CH_2-pyrazole), 22.35 (OCH_2CH_3), 13.94 ($ZnCH_2CH_3$), 12.97 (pyrazole-CH_3), 10.37 (pyrazole-CH_3), 0.48 ($ZnCH_2CH_3$). Anal. calcd. for $C_{20}H_{37}N_5OZn_2$ (494.32): C, 48.59; H, 7.54; N, 14.17; found: C, 48.36; H, 7.67; N, 14.35.

(b) NMR-Scale Generation of 12 from ZnEt(OEt) and 10. Complex **12** was also quantitatively generated in a Teflon-valved NMR tube by the reaction of ZnEt(OEt) (5.9 mg, 0.042 mmol) with complex **10** (15.0 mg, 0.042 mmol) in C_6D_6 (ca. 0.5 mL) at room temperature.

[Bis[2-(3,5-dimethyl-1-pyrazolyl)ethyl]amine]ZnEt(Cl) (13). To a solution of ZnEt(Cl), in situ generated from $ZnCl_2$ (117 mg, 0.86 mmol) and $ZnEt_2$ (106 mg, 0.86 mmol), in Et_2O (5 mL), was added **1** (225 mg, 0.86 mmol) in toluene (5 mL). The reaction mixture was stirred for 2 h at room temperature. After evaporation of volatiles under vacuum, the residue was recrystallized from pentane at −34 °C to give colorless crystals of **13** (0.290 g, 85%). ^{1}H NMR (THF-d_8): δ 5.87 (s, 2H, pyrazole-*H*), 4.28 (m, 4H, NCH_2CH_2-pyrazole), 3.24 (m, 4H, NCH_2CH_2-pyrazole), 2.28 (s, 6H, pyrazole-CH_3), 2.22 (s, 6H, pyrazole-CH_3), 1.11 (t, ^3J = 8.1, 3H, $ZnCH_2CH_3$), 0.06 (q, ^3J = 8.1, 2H, $ZnCH_2CH_3$). ^{13}C{^{1}H} NMR (THF-d_8): δ 148.59 (pyrazole-CCH_3), 141.44 (pyrazole-CCH_3), 105.03 (pyrazole-*C*H), 49.42 (NCH_2CH_2-pyrazole), 45.62 (NCH_2CH_2-pyrazole), 12.50 (pyrazole-CH_3),12.05 ($ZnCH_2CH_3$), 10.40 (pyrazole-CH_3), −0.85 ($ZnCH_2CH_3$). Anal. calcd. for $C_{16}H_{28}ClN_5Zn$ (391.27): C, 49.11; H, 7.21; N, 17.90; found: C, 49.63; H, 7.45; N, 17.98.

[Bis[2-(3,5-dimethyl-1-pyrazolyl)ethyl]amine]Zn($CH_2C_6H_4$-*p*-CH_3)(Cl) (14). The same procedure was used as that described for **13**, starting from **1** (180 mg, 0.69 mmol) and $ClZnCH_2$(*p*-$CH_3C_6H_4$) (1.38 mL of a 0.5 *M* solution, 0.69 mmol), to give **14** as colorless crystals (232 mg, 72%). A suitable crystal was selected for X-ray diffraction analysis. ^{1}H NMR (C_6D_6): δ 6.83 (d, ^3J = 7.5, 2H, Ph−H), 6.68 (d, ^3J = 7.5, 2H, Ph−H), 5.02 (s, 2H, pyrazole-*H*), 3.70 (m, 2H, NCH_2CH_2-pyrazole), 2.94 (m, 2H, NCH_2CH_2-pyrazole), 2.72 (m, 2H, NCH_2CH_2-pyrazole), 2.58 (m, 2H, NCH_2-CH_2-pyrazole), 2.38 (s, 6H, pyrazole-CH_3), 2.19 (s, 3H, CH_3Ph), 2.17 (s, 2H, *p*-CH_3PhCH_2), 1.60 (s, 6H, pyrazole-CH_3). ^{1}H NMR (THF-d_8): δ 6.61 (d, ^3J = 7.5, 2H, Ph−H), 6.44 (d, ^3J = 7.5, 2H, Ph−H), 5.84 (s, 2H, pyrazole-*H*), 3.85 (m, 4H, NCH_2CH_2-pyrazole), 3.04 (q, ^3J = 6, 4H, NCH_2CH_2-pyrazole), 2.24 (s, 6H, pyrazole-CH_3), 2.19 (s, 6H, pyrazole-CH_3), 2.09 (s, 3H, CH_3Ph), 1.58 (s, 2H, *p*-CH_3PhCH_2). ^{13}C{^{1}H} NMR (C_6D_6): δ 149.76 (Ph), 148.09 (pyrazole-CCH_3), 137.79 (pyrazole-CCH_3), 128.57 (Ph), 125.25 (Ph), 105.41 (pyrazole-*C*H), 48.71 (NCH_2CH_2-pyrazole), 45.25 (NCH_2CH_2-pyrazole), 20.67 (CH_3Ph), 13.48 (pyrazole-CH_3), 10.15 (pyrazole-CH_3). Anal. calcd. for $C_{22}H_{32}ClN_5Zn$ (467.37): C, 56.54; H, 6.90; N, 14.98; found: C, 56.08; H, 7.12; N, 15.37.

[Bis[2-(3,5-dimethyl-1-pyrazolyl)ethyl]amide]ZnCl (15). A Teflon-valved NMR tube was charged with **14** (50.0 mg, 0.110 mmol) and ca. 0.5 mL THF-d_8 was vacuum transferred in. The tube was sealed and kept at 80 °C for 2 days, resulting in the formation of **15** as a white precipitate. ^{1}H NMR (CD_2Cl_2): δ 5.89 (s, 2H, pyrazole-*H*), 4.31 (m, 2H, NCH_2CH_2-pyrazole), 3.24 (m, 2H, NCH_2CH_2-pyrazole), 2.30 (s, 6H, pyrazole-CH_3), 2.19 (s, 6H, pyrazole-CH_3).

Generation of [{Bis[2-(3,5-dimethyl-1-pyrazolyl)ethyl]amine}-Zn]$^+$[EtB(C_6F_5)$_3$]$^-$ (16). Complex **10** (14.9 mg, 0.042 mmol) and B(C_6F_5)$_3$ (21.3 mg, 0.042 mmol) were charged in a Teflon-valved NMR tube, and CD_2Cl_2 (ca. 0.5 mL) was vacuum transferred in. ^{1}H NMR spectroscopy was recorded, which revealed the quantitative formation of **16** within 10 min ^{1}H NMR (CD_2Cl_2): δ 6.16 (s, 2H, pyrazole-*H*), 4.26 (m, 2H, NCH_2CH_2-pyrazole, syn), 3.95 (m, 2H, NCH_2CH_2-pyrazole, anti), 3.50 (m, 2H, NCH_2CH_2-pyrazole, syn), 3.27 (m, 2H, NCH_2CH_2-pyrazole, anti), 2.31 (s, 6H, pyrazole-CH_3), 2.07 (s, 6H, pyrazole-CH_3). ^{13}C{^{1}H} NMR (CD_2Cl_2): δ 150.64 (pyrazole-CCH_3), 146.11 (pyrazole-CCH_3), 107.31 (pyrazole-*C*H), 53.87 (NCH_2CH_2-pyrazole), 47.11 (NCH_2CH_2-pyrazole), 12.55 (pyrazole-CH_3), 11.04 (pyrazole-CH_3). NMR data for EtB(C_6F_5)$_3^-$ anion: ^{1}H NMR (CD_2Cl_2): δ 1.16 (q br, ^3J = 6.0, 2H, BCH_2CH_3), 0.56 (t, ^3J = 6.0, 3H, BCH_2CH_3). ^{19}F NMR (CD_2Cl_2): δ −133.0 (d,$^3J_{F-F}$ = 22, 6F, *o*-F), −165.5 (t,$^3J_{F-F}$ = 22, 3F, *p*-F), −168.2 (t, ^3J = 22, 6F, *m*-F). ^{11}B NMR (CD_2Cl_2): δ −12.69 (s, BCH_2CH_3). ^{13}C{^{1}H} NMR (CD_2Cl_2): δ 148.2 (dm, J_{C-F} =233, *o*-C_6F_5B), 137.4 (dm, J_{C-F} =233, *p*-C_6F_5B), 136.2 (dm, J_{C-F} =233, *m*-C_6F_5B), 127.7 (C_{ipso}), 11.64 (CH_3CH_2B).

Solid-State Structure Determination of Complexes 2, 4, 6, 9−12, and 15. A suitable single crystal of **2**, **4**, **6**, **9**−**12**, and **15** was mounted onto a glass fiber using the "oil-drop" method. Diffraction data were collected at 100 K using a NONIUS Kappa CCD diffractometer with graphite monochromatized Mo Kα radiation (λ = 0.71073 Å). A combination of ω- and φ-scans was carried out to obtain at least a unique data set. Crystal structures were solved by means of the Patterson method, and the remaining atoms were located from difference Fourier synthesis, followed by full-matrix least-squares refinement on the basis of F^2 (programs Shelxs-97 and Shelxl-97).[22] Many hydrogen atoms could be found from the Fourier difference. Carbon-bound hydrogen atoms were placed at calculated positions and were forced to ride on the attached carbon atom. The hydrogen atom contributions were calculated but not refined. All non-hydrogen atoms were refined with anisotropic displacement parameters. The locations of the largest peaks in the final difference Fourier map calculation as well as the magnitude of the residual electron densities were of no chemical significance. Crystal data and details of data collection and structure refinement are given in Table 1 and Table 2. Crystallographic data for **2**, **4**, **6**, **9**−**12**, and **15** are also available as cif files (see Supporting Information).

Typical Procedure for MMA or *rac*-Lactide Polymerization. To a 10-mL flask equipped with a magnetic stirrer, containing the catalyst (0.05 mmol) in toluene (or THF or CH_2Cl_2) solvent, was introduced Li-enolate, MAD, or B(C_6F_5)$_3$ (for MMA polymerization) in toluene (or THF or CH_2Cl_2) solvent. Then, the proper

(22) (a) Sheldrick, G. M. *SHELXS-97, Program for the Determination of Crystal Structures;* University of Goettingen: Goettingen, Germany, 1997. (b) Sheldrick, G. M. *SHELXL-97, Program for the Refinement of Crystal Structures*; University of Goettingen: Goettingen, Germany, 1997.

amount of monomer (MMA or *rac*-Lactide) was rapidly added. The polymerization was carried out for a time period. The reaction was then quenched by addition of acidified methanol (3% HCl, 200 mL). The precipitated polymer was filtered and dried overnight under vacuum at 60 °C.

Acknowledgment. We thank Total and Arkema Co. (grant to B. L.) and the Centre National de la Recherche Scientifique for financial support of this work. We gratefully thank Dr. C. Navarro, Dr. M. Glotin, and Dr. G. Meunier (Arkema Co.) for valuable discussions.

Supporting Information Available: Crystallographic data for **2**, **4, 6**, **9**−**12**, and **15** as CIF files. This material is available free of charge via the Internet at http://pubs.acs.org

IC061749Z